



**HAL**  
open science

## Variational data assimilation to improve subsurface drainage model parameters

Samy Chelil, Hind Oubanas, Hocine Henine, Igor Gejadze, Pierre Olivier Malaterre, Julien Tournebize

► **To cite this version:**

Samy Chelil, Hind Oubanas, Hocine Henine, Igor Gejadze, Pierre Olivier Malaterre, et al.. Variational data assimilation to improve subsurface drainage model parameters. *Journal of Hydrology*, 2022, 610, pp.128006. 10.1016/j.jhydrol.2022.128006 . hal-03700970

**HAL Id: hal-03700970**

**<https://hal.science/hal-03700970>**

Submitted on 22 Jul 2024

**HAL** is a multi-disciplinary open access archive for the deposit and dissemination of scientific research documents, whether they are published or not. The documents may come from teaching and research institutions in France or abroad, or from public or private research centers.

L'archive ouverte pluridisciplinaire **HAL**, est destinée au dépôt et à la diffusion de documents scientifiques de niveau recherche, publiés ou non, émanant des établissements d'enseignement et de recherche français ou étrangers, des laboratoires publics ou privés.



Distributed under a Creative Commons Attribution - NonCommercial 4.0 International License

# Variational Data Assimilation to Improve Subsurface Drainage Model

## Parameters

Samy CHELIL<sup>1</sup>, Hind OUBANAS<sup>2</sup>, Hocine HENINE<sup>1</sup>, Igor GEJADZE<sup>2</sup>, Pierre Olivier MALATERRE<sup>2</sup> and Julien TOURNEBIZE<sup>1</sup>

<sup>1</sup> University of Paris-Saclay, INRAE Jouy-en-Josas - Antony, UR HYCAR, Antony, France

<sup>2</sup> G-EAU, Univ Montpellier, AgroParisTech, BRGM, CIRAD, IRD, INRAE, Institut Agro, Montpellier, France

**Corresponding author:** Samy CHELIL (samy.chelil@inrae.fr)

### Abstract

Variational data assimilation (VDA) has been implemented to enhance the estimation of the unknown input parameters of a new agricultural subsurface drainage model (SIDRA-RU) through assimilating drainage discharge observations. The adjoint model of SIDRA-RU has been successfully generated through the generic automatic differentiation tool (TAPENADE). First, the adjoint model is used to explore the local and global adjoint sensitivities of the valuable function defined over the drainage discharge simulations with respect to model input parameters. Next, the most influential parameters are estimated by applying the Variational DA approach. The performed sensitivity analysis shows that the most influential parameters on drainage discharge are those controlling the dynamics of the water table; the second most influential parameters manage the drainflow start of each drainage season. Compared to an alternative gradient-free calibration performance, the estimation of these governing parameters by the variational method improves the overall quality of the drainage discharge prediction, in particular in terms of the cumulative water volume. Improved parameters

23 generate less than 5 mm (1%) of the discrepancy between simulated and observed water  
24 volumes, based on the five years of daily discharge observations on the Chantemerle  
25 agricultural parcels (36 ha). Preliminary numerical tests have shown the potential presence of  
26 multiple local minima, thus pointing out the equifinality issues. The latter can be highlighted  
27 by the self-compensation of both the physical soil parameters and the main conceptual  
28 parameters. For improving the robustness of the parameter estimates, a novel hybrid  
29 “Bayesian Variational” method is suggested. This method is based on the Bayesian averaging  
30 of an ensemble of optimal estimates.

31

32 **Keywords:** agricultural drainage model, adjoint sensitivity analysis, variational data  
33 assimilation, Bayesian estimation.

## 34 1. INTRODUCTION

35 Agricultural drainage systems are designed to remove the excess water within soils subjected  
36 to frequent and continuous waterlogging, in particular during the winter season. The  
37 agricultural subsurface drained areas contribute to 10% of French arable soils (Vincent,  
38 2020). The main objectives of agricultural drainage are to ensure better crop yields  
39 (Mohtadullah, 1990) and facilitate grazing and access to cultivated fields by farmers.  
40 Subsurface drainage flow only occurs when the perched water table rises above the drain  
41 depth, as identified by “drainage season”. Three drainage patterns can be distinguished during  
42 an agricultural drainage season (Lesaffre, 1988): (1) the “pre-flow drainage stage”, consists  
43 of a gradual saturation of the soil and a limited flow into drains; (2) the “intensive drainage  
44 stage” (IDS) featuring a continuous and rapid reaction to each rainfall event; (3) the “drying  
45 stage”. The latter is characterized by the water flow decrease until the drainage flow stops  
46 during summer.

47 The hydrological behavior of agricultural drainage networks is highly dependent on  
48 hydrometeorological data and soil hydro-physical properties. To understand the hydrology of  
49 drained agricultural lands, several numerical models have been developed to approximate the  
50 underlying dynamics and physical processes. The appropriate modeling of the perched water  
51 table formed in drained soils is complex, time-consuming and still require multiple input data  
52 and parameters. In contrast, some simplified models simulate the outputs from a limited input  
53 dataset but are not able to describe the physics of hydrological and hydraulic processes  
54 (Tournebize et al., 2004; Henine et al., 2010; Henine et al., 2014).

55 Several models are reported in the literature (Gurovich and Oyarce, 2015) for designing  
56 drainage networks and monitoring hydraulic patterns. DRAINMOD (Skaggs et al., 2012),  
57 EnDrain (Valipour, 2012), CSUID (Alzraiee et al., 2013), and SIDRA that was initially  
58 developed at INRAE (formerly Cemagref) by Lesaffre (1988) describe the hydrological and  
59 hydraulic behavior of drained agricultural lands. More specifically, SIDRA (SIMulation of  
60 DRAINage) model simulates water table variations at the mid-drain and calculates discharge  
61 at the drainage network outlet. Since that time, several model improvements have been  
62 proposed by Bouarfa (1995) and Bouarfa and Zimmer (2000), including a better  
63 consideration of the evaporation term and the water table shape. Recently, a new conceptual  
64 module has been introduced to manage the quantity of water seeping through the vadose soil  
65 zone (Jeantet et al., 2021; Henine et al., 2022), referred to as SIDRA-RU (RU “Réserve  
66 Utile” for Water Holding Capacity).

67 Furthermore, the model uncertainty management is indispensable to enhance the hydrological  
68 prediction (Blöschl et al., 2019). Leaving out the structural uncertainty specific to each  
69 model, one can focus on improving the input/parameter estimation. This could be achieved in  
70 part by considering the most suitable optimization approach in terms of uniqueness,  
71 robustness and stability of the final solution.

72 It is known that long-term discharge predictions are needed to adapt and prepare agricultural  
73 lands to cope with the effects of climate change (Jiang et al., 2020; Golmohammadi et al.,  
74 2021). Unlike the short-range predictions (e.g. days, weeks), which may require the  
75 knowledge of the hydrological state at the beginning of the prediction window (e.g. flood  
76 forecasting), the long-range predictions are almost fully defined by the driving conditions  
77 (anticipated rainfall and evapotranspiration) and the model parameters. That is why this paper  
78 focuses on solving a classical parameter estimation (calibration) problem for SIDRA-RU  
79 model, using observations of drainage discharge recorded before the prediction window.

80 First, the most influential model parameters on model outputs should be identified. This can  
81 be achieved through the Sensitivity Analysis (SA), a key preliminary step to the optimization  
82 exercise (Stange et al., 2000; Migliaccio and Chaubey, 2005; Razavi et al., 2021). Several  
83 approaches can be employed in local and global SA, including variance-based approaches  
84 (Sobol, 1993; Saltelli, 2002) and derivative-based methods (Cacuci, 1981; Morris, 1991). The  
85 adjoint sensitivity analysis involves a simultaneous computation of all sensitivities using  
86 adjoint operators within a single model run. In addition, inequality links have been  
87 established between the derivative-based global sensitivity measures (DGSM) and Sobol's  
88 indices, thus yielding SA for a large number of input parameters (Kucherenko, 2009;  
89 Lamboni et al., 2013). In the same context, Gejadze et al. (2019) derived a generalized  
90 relationship between the global sensitivity indices and the Polynomial Chaos coefficients,  
91 making SA suitable for high-dimensional models.

92 Once the most influential parameters are identified, one can estimate their values using the  
93 available observations. Several approaches are presently available, ranging from the PAP-GR  
94 Michel's calibration algorithm (Michel, 1989) highlighted by Mathevet (2005), to more  
95 sophisticated Data Assimilation (DA) methods, such as the Kalman filter and its ensemble

96 variants, Particle filters, variational Data Assimilation (VDA) and hybrid methods  
97 (Abbaszadeh et al., 2019).

98 In particular, VDA method is preferred in operational geophysical large-scale applications,  
99 due to its scalability, robustness and potential to handle nonlinear systems under high  
100 uncertainty (Courtier et al., 1998; Fischer et al., 2005; Gauthier et al., 2007). However,  
101 references on the application of VDA to hydrological models remain relatively scarce. In  
102 recent studies, the optimal estimates of the unknown model variables and/or parameters have  
103 been obtained via minimization of a cost function using the gradient-based methods (Nguyen  
104 et al., 2016; Oubanas et al., 2018; Ghorbanidehno et al., 2020; Jay-Allemand et al., 2020).  
105 This procedure requires developing the adjoint counterpart of the model, which could be  
106 challenging to obtain in some cases (e.g. presence of non-differentiable operators).  
107 Application of filtering methods is natural for solving the state or state-parameter estimation  
108 problems to enable the short and medium range state forecasting. For the pure calibration  
109 problems the ‘full sample’ data processing approach such as VDA should be preferred, given  
110 the adjoint model is available.

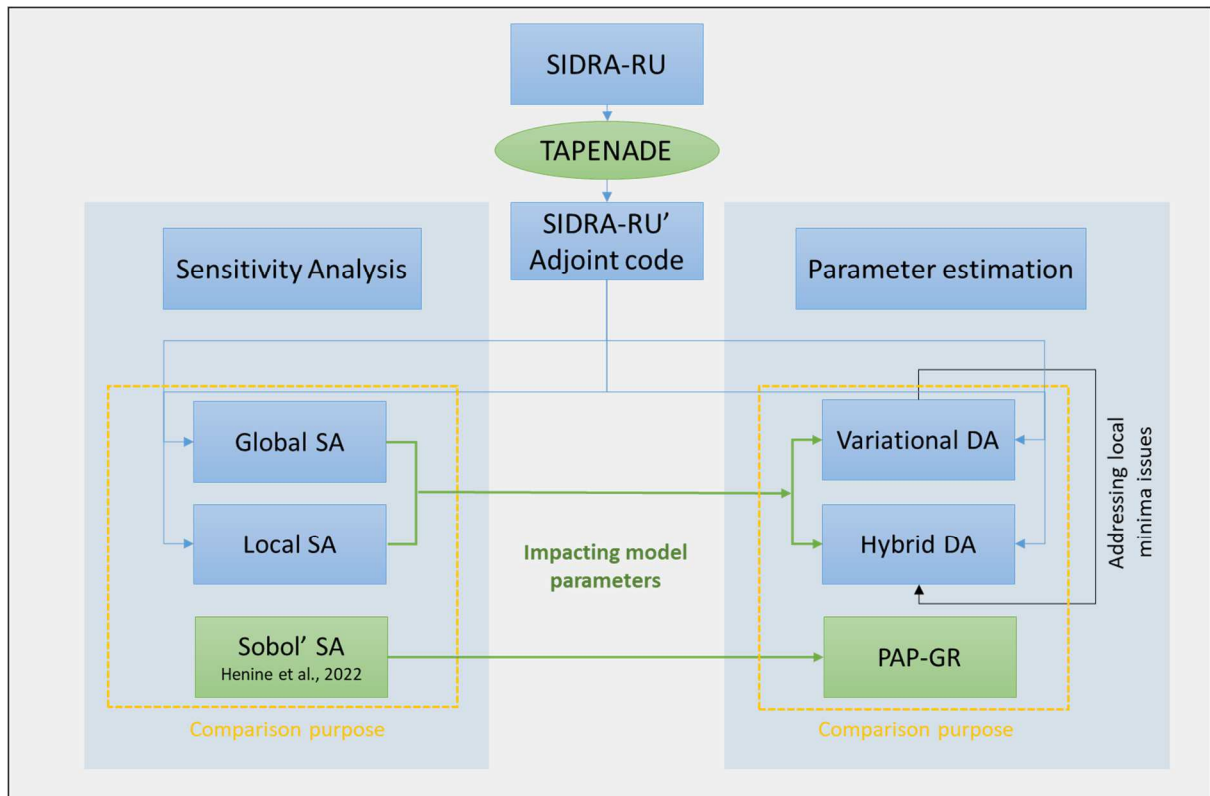
111 A common issue when solving ill-posed problems in a variational formulation using the  
112 gradient-based minimization is the likely presence of multiple local minima in the cost  
113 function (Dennis and Moré, 1977). A comparison between different optimization algorithms  
114 applied to hydrological models was presented by Arsenault et al. (2014). Some of these  
115 methods can be highly sensitive to the choice of the initial guess, known as the “background”  
116 in DA or the “prior” in statistics. This finding was supported by Pan and Wu (1998), in which  
117 an original approach based on the simplex method was used to reveal and avoid the  
118 convergence to local minima. Furthermore, Skahill and Doherty (2006) proposed a simple  
119 methodology to address the local minima issue. Based on a local search algorithm, their  
120 methodology consists of starting the minimization process with different parameter values to

121 increase the probability of reaching the global minima. The same concept has been deployed  
122 when calibrating 3D morphodynamic model data (Shoarinezhad et al., 2020) using the PEST  
123 parameter estimation package (Welter et al., 2012), thus showing that the optimization  
124 process is substantially affected by the local minima issue.

125 However, the presence of multiple local minima is, essentially, a sign of ill-posedness in  
126 terms of non-uniqueness (equifinality thesis, Beven (2006)). In these circumstances, one  
127 should look for the mean of the posterior distribution rather than for one of its modes. The  
128 posterior mean is a natural output of the Bayesian methods. Since the direct use of these  
129 methods may be difficult in high dimensions, we suggest a simple hybrid approach referred  
130 below as the Bayesian Variational (BV) method. That is, the mean is computed over an  
131 ensemble of parameter estimates obtained by the variational method, whereas each ensemble  
132 member is weighed by the corresponding likelihood. The method is described in detail in  
133 Section 2.4.2.

## 134 **2. MATERIALS AND METHODS**

135 This paper focuses on improving the long-range predictive performance of the SIDRA-RU  
136 model (Henine et al., 2022) that runs with a daily time step and requires knowledge of the  
137 rainfall, potential evapotranspiration and a set of model parameters. First, the adjoint local  
138 and global sensitivity analysis are performed, in accordance with the methodologies  
139 presented in Goutal et al. (2018) and Gejadze et al. (2019). Next, the VDA method is applied  
140 to improve the estimation of the most influential model parameters. Therefore, the uniqueness  
141 (equifinality) of the parameter estimation problem is investigated by running the ensemble of  
142 minimizations from different starting points. Then, the hybrid BV method is performed to  
143 improve the robustness of the estimates. A flowchart is embedded below to indicate the  
144 connections between the methodology elements (Figure 1).

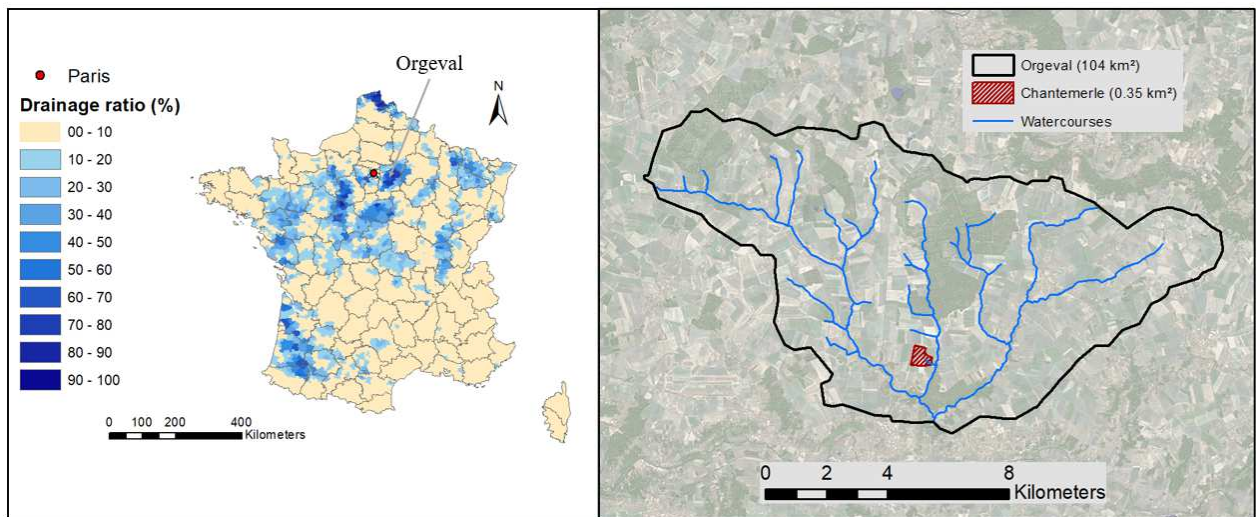


145

146 **Figure 1.** A flowchart clarifying connections existing between the methodology elements

147 **2.1. Study area description and data**

148 The Chantemerle agricultural sub-catchment (36 ha) has been considered for this study. The  
 149 field includes a set of artificially drained agricultural parcels. On average, the drains are laid  
 150 at a depth of 0.9 m and spaced by 10 to 12 meters. The study area is located in Aulnoy  
 151 (“*Seine et Marne*” department; 70 km east of Paris), within the Orgeval catchment (Tallec  
 152 (2012); Figure 2).



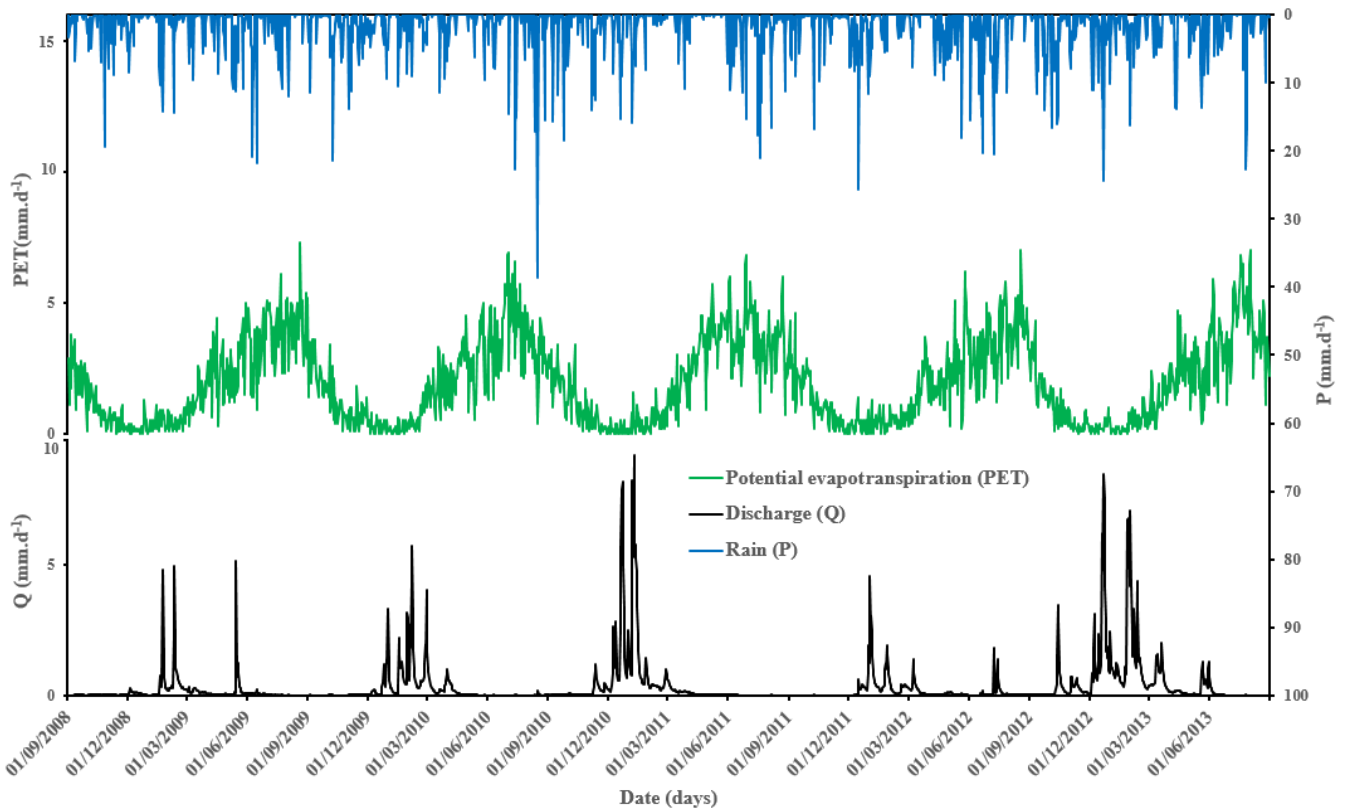
153

154 **Figure 2.** The “Chantemerle” agricultural field and its general location (48°50' N, 3° 6' E),  
 155 “Seine et Marne department”, France)

156 The study site experiments are operated by the GIS-ORACLE research observatory  
 157 (<https://gisoracle.inrae.fr/>). The soil is luvisol type (FAO, 2006; Tournebize et al., 2015) with  
 158 a silty texture (mixture of sand and clay), which is belong to the Aqualf suborder following  
 159 the US taxonomy system. This type of soil gives rise to a temporary water table, causing fast  
 160 and continuous water flows during wet periods. The outlet of the subsurface drainage  
 161 network has been monitored by the water level measurement device (SE-200 OTT). Then, the  
 162 water level has been transformed into discharge value using calibrated rating curve. The  
 163 rainfall has been measured near the study site using a rain gauge. Daily potential  
 164 evapotranspiration (PET) data have been extracted from the SAFRAN database (Vidal et al.,  
 165 2010). PET values have been calculated according to the Penman-Monteith formula.  
 166 Available data cover September 1<sup>st</sup>, 2008 to August 31<sup>st</sup>, 2013 (Figure 3).

167 Among all recorded data, two wet hydrological years, 2010/2011 and 2012/2013 can be  
 168 distinguished, accumulating respectively 172 mm and 217 mm of drained water. The three  
 169 remaining dry years account for a combined 209 mm, nearly equal to the drained water

170 accumulated in just a single wet season. This contrast in the quantity of drained water (i.e.  
171 succession of dry and wet seasons) lends more reliability to our results.



172

173 **Figure 3.** Five years (2008-2013) of daily drainage discharge data (Q, black) and rainfall (P,  
174 blue) recorded at the “Chantemerle” field scale. The related daily potential evapotranspiration  
175 values (PET, green) are extracted from the SAFRAN database.

## 176 2.2. The SIDRA-RU model

177 SIDRA-RU is a semi-analytical and semi-conceptual model, which is run at the scale of  
178 agricultural plots with a daily time step. The model is based on three coupled modules  
179 (Figure 4; Henine et al. (2022)):

- 180 - The first module estimates the net infiltration based on more realistic  
181 evapotranspiration, referred to herein as corrected evapotranspiration (CET). This  
182 variable takes into account the potential evapotranspiration rate (PET), the available  
183 soil water content in the soil reservoir, and the crop coefficient ( $\beta$ ). The net infiltration

184 is calculated as the difference between the precipitation ( $P$ ) and the CET (Appendix  
185 A; formulas A.1).

186 - Based on a conceptual reservoir approach, the second module calculates the net  
187 recharge to the perched water table as a function of the actual water level in the soil  
188 reservoir ( $S(t)$ ). Three distinct soil reservoir thresholds are accordingly defined  
189 namely minimum ( $S_{\min}$ ), intermediate ( $S_{\text{inter}}$ ) and maximum ( $S_{\max}$ ). When  $S(t)$  lies  
190 between  $S_{\text{inter}}$  and  $S_{\max}$ , the model splits the net infiltration rate into two components  
191 via partition parameter ( $\alpha$ ). The first part ( $\alpha$ ) recharges the water table ( $R$ ) while the  
192 second part ( $1-\alpha$ ) continues to fill the soil reservoir. When  $S(t)$  reaches the maximum  
193 level ( $S_{\max}$ ), the entire net infiltration recharges the water table (Appendix A; formulas  
194 A.2). It is worthwhile to note that  $S(t)$  level at the beginning of the hydrological year  
195 ( $N$ ) is based on the soil saturation degree of the year ( $N-1$ ).

196 - The third module simulates drainage discharge ( $Q$ ) and the mid-drain water table  
197 height ( $h$ ) above drain by applying the SIDRA model (Lesaffre, 1988). Note that  $Q$   
198 and  $h$  values are calculated considering the Hooghoudt equation (Hooghoudt, 1940)  
199 (Appendix A; formulas A.3).

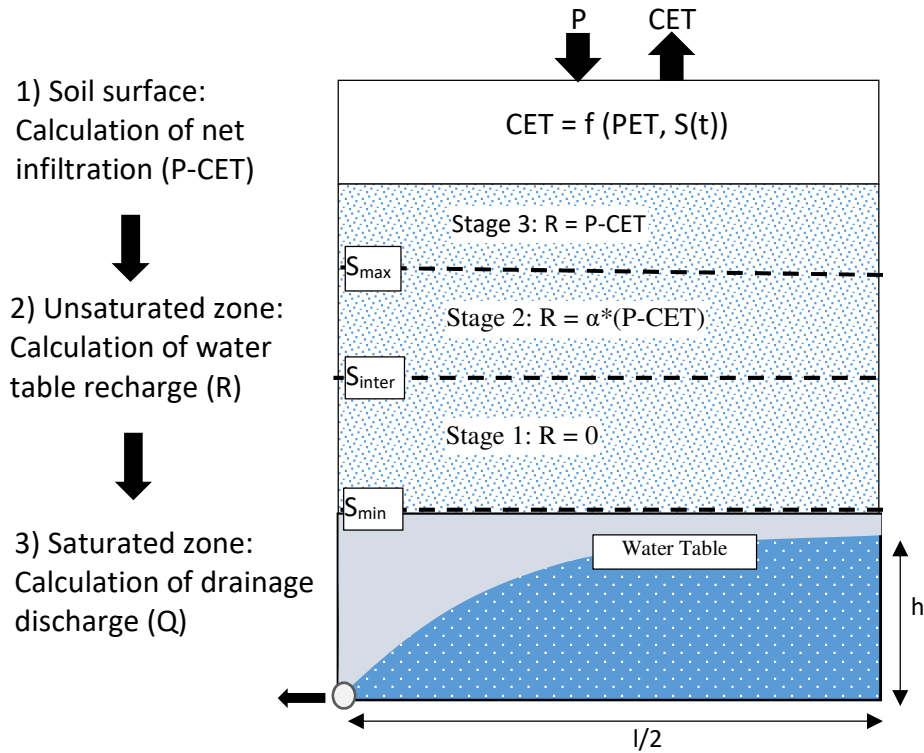


**Figure 4.** Diagram presenting the three SIDRA-RU modules (Henine et al., 2022)

SIDRA-RU inputs are precipitation ( $P$ ) and potential evapotranspiration data ( $PET$ ), both considered as forcing variables, along with the model parameters to simulate the mid-drain water level variations ( $h$ ) and drainage discharges ( $Q$ ) outputs (Figure 4). The model contains two state variables  $h(t)$  and  $S(t)$ , and eleven parameters.

The parameter set of the model is listed in Table 1. This set includes the SIDRA model parameters ( $K_{sat}$  and  $\mu$ ) and the two soil reservoir parameters, i.e., intermediate soil reservoir level ( $S_{inter}$ ) and reservoir storage capacity during the intensive drainage season ( $SSDI$ ) which is equal to the difference between  $S_{max}$  and  $S_{inter}$ . The remaining parameters are considered as either given invariants, regardless of field characteristics, or typical invariant characteristics at the field scale. It should be pointed out that the presence of an impermeable layer, on which the drains are laid, limits deep infiltrations (aspect not considered herein). In addition, Augéard et al. (2005) showed that surface runoff becomes negligible under the same

214 field conditions since the agricultural plots are being extensively drained, which leads to  
 215 infrequent soil overflow.

216 **Table 1.** Classification of SIDRA-RU parameters

Type	Parameters	Unit	Notes
SIDRA model	Saturated hydraulic conductivity ( $K_{sat}$ )	m/day	Measurable but often inaccessible
	Drainage porosity ( $\mu$ )	(-)	
	Water table shape coefficients (A and C)	(-)	Fixed model parameters
Drainage design	Parcels area (S)	m <sup>2</sup>	Values usually known and dependent on the studied field
	Drain spacing (l)	m	
	Drain depth (P)	m	
Evapotranspiration correction	Crop coefficient ( $\beta$ )	(-)	Internal parameters
Soil reservoir	Water share coefficient ( $\alpha$ )	(-)	Not measurable at the field scale
	Intermediate threshold ( $S_{inter}$ )	mm	
	Reservoir storage capacity (SSDI)	mm	

217 **2.3. Adjoint sensitivity analysis**

218 In addition to the climate data of rainfall and potential evapotranspiration, SIDRA-RU  
 219 features 11 input parameters (Table 1), some of which are difficult to assess directly, such as  
 220 SIDRA and soil reservoir parameters. In order to reveal the most important parameters to be  
 221 estimated, a sensitivity analysis (SA) is initially performed. Next, the chosen parameters form  
 222 the control vector to be estimated using the data assimilation method (see Section 2.4).

223 The present paper investigates both local and global adjoint sensitivities. The latter are  
224 computed using the derivative-based approaches involving the SIDRA-RU adjoint model to  
225 evaluate the gradient of a valuable function  $J$ , defined over the model response. Note that the  
226 formulation of  $J$  depends on the purpose of the study.

227 The adjoint model is generated using the automatic differentiation (AD) tool TAPENADE  
228 (Hascoet and Pascual, 2013), developed at Inria (<https://team.inria.fr/ecuador/en/tapenade/>).

229 The AD engine processes the Fortran code which implements the mapping from the model  
230 inputs to the valuable function  $J(U)$ . For the AD procedure to succeed, one has to ensure that  
231 all operators of the code are differentiable. This is not always the case, especially with  
232 conceptual models. For example, the flow routing scheme originally used in AIGA model  
233 (described in Jay-Allemand et al. (2020)) was not differentiable. Since the need for a more  
234 accurate routing scheme was obvious, the new one has been developed taking into account  
235 the differentiability requirement. Concerning SIDRA-RU model, a brief inspection of the  
236 model equations (see Appendix A) shows that it is conditionally differentiable. Here,  
237 ‘conditionally’ means that all parameters are explicitly involved inside the continuous  
238 operators, so the gradient with respect to all parameters does exist. However, some  
239 parameters and state variable  $S(t)$  are involved as arguments in the logical expressions (if-  
240 then/elseif-then/endif), which are not differentiable. This means that the computed gradient is  
241 approximate since it does not include the component associated to the unaccounted graphs. In  
242 practice, this component is usually quite small in comparison to the explicit component and,  
243 therefore, does not affect the minimization result significantly. To check this, any logical  
244 expression can be substituted with the numerical one using the logistic function  $H(x) =$   
245  $1/(1 + e^{-2kx})$ , where  $k$  is a big enough real. Since the exponent is a computationally  
246 expensive function, one has to keep a compromise between the gradient accuracy and the

247 computational cost in the modified version of the code. Concerning SIDRA-RU model, no  
248 modifications have been considered as necessary.

### 249 **2.3.1. Local adjoint sensitivity analysis (LASA)**

250 Let us consider a model  $M$  that transforms input vector  $I$  into model output vector  $X$ :

$$251 \quad M(I) = X \quad (1)$$

252 In the particular case of the SIDRA-RU model, input vector  $I$  includes the vector of  
253 parameters  $U_i$  and the climate forcing datasets (i.e. rainfall and potential evapotranspiration):

$$254 \quad I = \{P(t), PET(t), U\} \quad (2)$$

255 In this study, rainfall  $P$  and evapotranspiration  $PET$  are considered to be known with high  
256 accuracy; thus, their values are not estimated. The input parameters vector  $U$  is defined as  
257 follows:

$$258 \quad U = \{S, l, K_{sat}, \mu, A, C, P, S_{inter}, SSDI, \alpha, \beta\} \quad (3)$$

259 Where:  $SSDI = S_{max} - S_{inter}$

260 The model response  $X$  represents the simulated temporal evolution of drainage discharge  $Q$ :

$$261 \quad X = Q(t) \quad t \in [0, T] \quad (4)$$

262 Since in the current SA framework the model output is directly and completely observed, no  
263 observation operator is required, and the corresponding observations are hereafter  
264 denoted  $X^*$ .

265 In the local SA context, the sensitivity of the model response with respect to inputs is  
266 quantified locally around a given point. Since the true value of  $U$  is unknown, it is typically  
267 substituted by a prior  $U_b$ , where index “b” stands for the “background” information in DA.

268 Reasonable initial guess of  $U$  can be provided by an expert evaluation or through introducing  
269 a pre-calibration step.

270 Adjoint SA method computes the sensitivity of the model response  $X$  with respect to the  
271 model inputs  $U$  via the gradient of the valuable function  $J(X(U)) := J(U)$  at the point  $U_b$   
272 (background value):

$$273 \quad \frac{\partial J(U_b)}{\partial U} = \left( \frac{\partial J(U_b)}{\partial U_1}, \dots, \frac{\partial J(U_b)}{\partial U_n} \right) \quad (5)$$

274 All components of the gradient are computed simultaneously using a single adjoint model  
275 run, which is the main advantage of the adjoint approach as compared to the finite-difference  
276 or statistical methods. Moreover, the derivative obtained is exact (up to the machine  
277 accuracy, if all operators involved are differentiable), rather than a finite-difference  
278 approximation.

279 Next, the gradient components must be properly scaled to construct the local sensitivities  
280 meaningful in terms of the Analysis of Variance (ANOVA) approach. Let us consider a  
281 Gaussian perturbation  $\xi \sim N(0, B)$ , where  $B = \text{diag}(\sigma_i^2), i = 1, \dots, N$  and  $\sigma_i$  is the standard  
282 deviation. It can be seen that

$$283 \quad \text{Var}[J] = E \left[ (J(U_b + \xi) - J(U_b))^2 \right] = \sum_{i=1}^N \left( \sigma_i \frac{\partial J(U_b)}{\partial U_i} \right)^2 \quad (6)$$

284 It follows from the above formula that each component of the gradient  $\partial J(U_b)/\partial(U_i)$  has to  
285 be scaled by the corresponding  $\sigma_i$ .

286 In this study, the Kling-Gupta Efficiency (KGE, Gupta et al. (2009)) has been chosen as a  
287 valuable function  $J(U)$ . KGE is widely used to assess the performance of hydrological  
288 models and improve simulation quality (Pechlivanidis et al., 2011; Patil and Stieglitz, 2015;  
289 Haas et al., 2016; Santos, 2018). The KGE metric ranges from  $-\infty$  to 1, where 1 corresponds  
290 to the best match between simulations and observations.

291 
$$J(X, X^*) = 1 - \sqrt{(r - 1)^2 + (d - 1)^2 + (m - 1)^2} \quad (7)$$

292 where:

293 -  $m = \frac{\bar{X}}{\bar{X}^*}$ : the ratio between the mean of the simulated and observed data.

294 -  $r = \frac{\sum_{i=1}^n (X_i - \bar{X})(X_i^* - \bar{X}^*)}{\sqrt{\sum_{i=1}^n (X_i - \bar{X})^2} \sqrt{\sum_{i=1}^n (X_i^* - \bar{X}^*)^2}}$ : the Pearson correlation coefficient.

295 -  $d = \frac{\bar{X}^* \sqrt{\sum_{i=1}^n (X_i - \bar{X})^2}}{\bar{X} \sqrt{\sum_{i=1}^n (X_i^* - \bar{X}^*)^2}}$ : the ratio between the standard deviation of simulated and  
 296 observed values.

297 Moreover, the use of KGE allows the performance of adjoint-based and Sobol methods  
 298 (Sobol, 1993) to be compared. The latter had recently been explored in (Henine et al., 2022).

### 299 **2.3.2. Global adjoint sensitivity analysis (GASA)**

300 While the local SA answers how a small perturbation around the background value  $U_b$   
 301 influences the model response  $X$ , the global SA focuses on the model output variance or,  
 302 more precisely, on how the input variability influences the output variance. The global SA  
 303 reveals which parts of the output variance are due to different inputs by estimating Sobol  
 304 indices, which are a central tool (and key point) since they provide a quantitative and rigorous  
 305 overview of the influence of inputs on the model response. The commonly used global SA  
 306 method is the variance-based ANOVA decomposition. This paper introduces the adjoint-  
 307 based global SA described in (Gejadze et al., 2019), featuring a methodology that derives a  
 308 generalized relationship between the global sensitivity indices and the Polynomial Chaos  
 309 coefficients.

310 The variability of inputs is represented by a sample of random vectors from a given  
 311 probability distribution. For example, one can consider the Gaussian distribution using the

312 background vector  $U_b$  as its mode. Since in our case the informative priors for  $U$  are either  
 313 not available or not accurate enough, we use the uniform distribution to define a random  
 314 sample within a defined interval  $[a_i, b_i]$  for each element of  $U$ , as follows:

$$315 \quad \begin{aligned} \xi_i &\sim u(a_i, b_i) \\ \xi_i &= (b_i - a_i) * \varepsilon_i + a_i \end{aligned} \quad , \quad \varepsilon_i \sim u(0,1) \quad (8)$$

316 The bounds  $a$  and  $b$  are specified for all SIDRA-RU parameters. The choice of the uniform  
 317 distribution overcomes the need for background  $U_b$  and, subsequently, for the pre-calibration  
 318 step.

319 The sample size is chosen by taking into account the computational requirements and model  
 320 complexity into account. Since the SIDRA-RU is relatively inexpensive, it is feasible to use a  
 321 relatively large sample size, which can be chosen to compromise between the stability of the  
 322 sensitivities and CPU time.

323 In this paper, we only consider the first-order ‘main-effect’  $S_i$  indices as well as the ‘total-  
 324 effect’  $S_i^T$  indices (Saltelli, 2002), defined as follows:

$$325 \quad \begin{cases} S_i = \frac{\text{var}(E[J(\xi)|\xi_i])}{\text{var}(J(\xi))} \\ S_i^T = \frac{\text{var}(J(\xi)) - \text{var}(E[J(\xi)|\xi_{-i}])}{\text{var}(J(\xi))} \end{cases} \quad (9)$$

326 Where  $J(\xi)|\xi_i$  represents the random value of  $J$ , with the input component  $\xi_i$  being fixed at  
 327 its generic value;  $\xi_{-i}$  stands for ‘all, but i’, and  $\text{Var}(J(\xi))$  is the total variance of  $J(\xi)$ .

328 While the main-effect indices, which are commonly used in ANOVA analysis, quantify the  
 329 single influence of individual variables or some groups of variables, the total-effect indices  
 330 measure the influence of a variable jointly with all its interactions with other variables.  
 331 Alternatively, these indices can be viewed as a measure of the variability remaining to the  
 332 output when all but one input variables are fixed. If the total sensitivity index of a variable is

333 sufficiently small, this variable can be removed from further analysis, because neither the  
 334 variable nor any of its order interactions have an impact on the valuable function. Thus, the  
 335 total sensitivity index can be used to detect the essential variables for the calibration process.

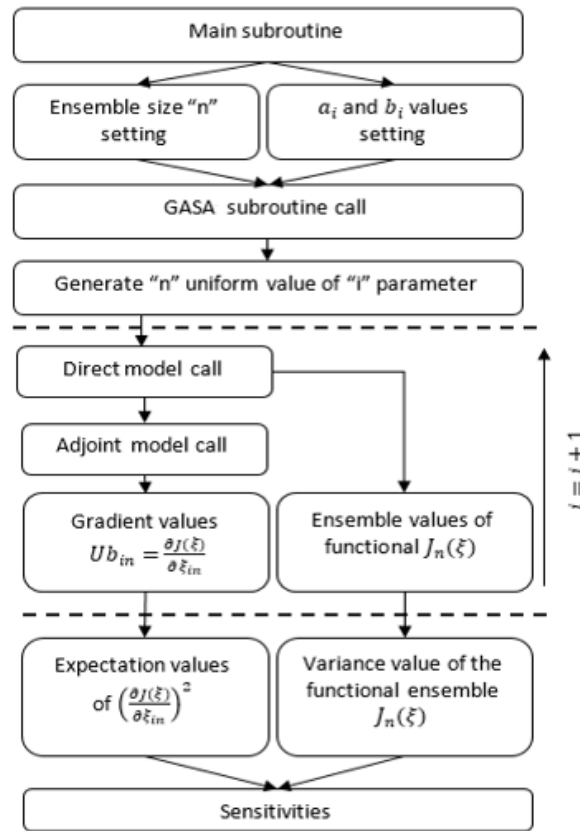
336 The methodology presented in Gejadze et al. (2019) suggests a generalized approximation for  
 337 the upper bound of the total-effect indices  $S_i^T$  based on a computation of the derivative of the  
 338 valuable function  $J$ . We limit ourselves here to the first-order analysis. Future work will  
 339 investigate the approximation of  $S_i^T$  in considering second-order interactions. Given that  $\xi$  is  
 340 a vector constituted of independent and identically distributed normal random variables, the  
 341 following estimate holds:

$$342 \quad S_i^T \text{Var}(J(\xi)) \leq E \left[ \left( \frac{\partial J(\xi)}{\partial \xi_i} \right)^2 \right] \quad (10)$$

343 In the case of independent uniformly distributed variables defined over the interval  $[a_i, b_i]$   
 344 (Lamboni et al., 2013), the following can be written:

$$345 \quad S_i^T \text{Var}(J(\xi)) \leq E \left[ \left( \frac{\partial J(\xi)}{\partial \xi_{in}} \right)^2 \right] \left( \frac{b_i - a_i}{\pi} \right)^2 \quad (11)$$

346 Similarly, we employ the same formulation of the valuable function introduced in Section  
 347 2.3.1. The gradient of  $J$  within the GASA framework is computed using automatic  
 348 differentiation. A detailed algorithm of the GASA applied to the SIDRA-RU model is  
 349 described in Figure 5.



350

351

**Figure 5.** Simplified version of the global adjoint SA algorithm

352

#### 2.4. Variational data assimilation algorithm

353

Data assimilation methods are widely used in the geophysical sciences (Reichle, 2008). These

354

methods provide the best possible estimates of unknown model inputs (initial and driving

355

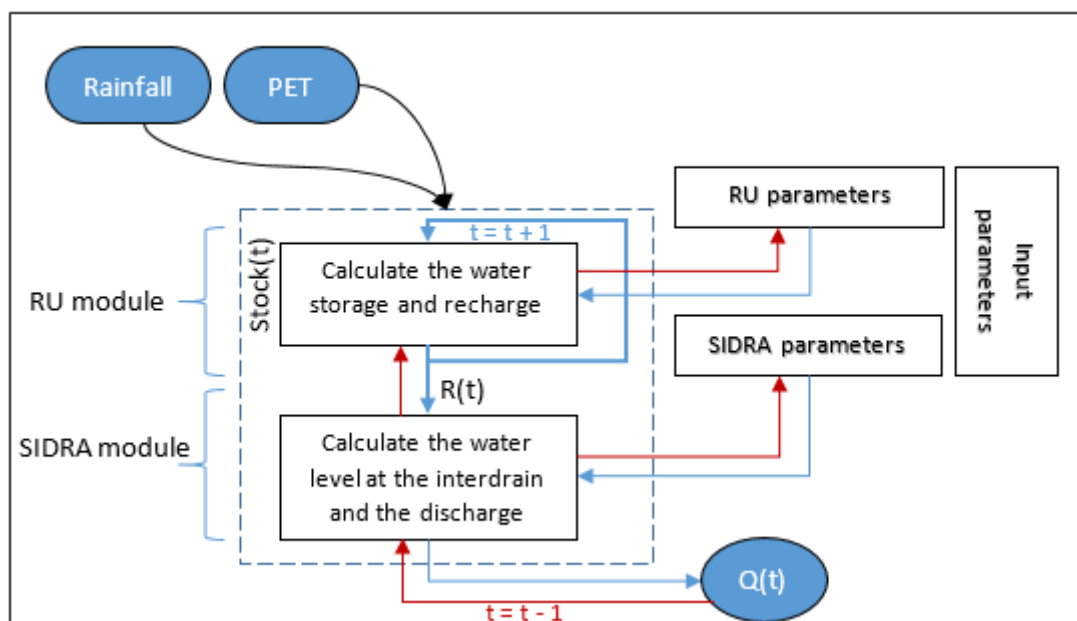
conditions, parameters) by combining all available information: observations, *a priori* data

356

(coming from expertise or preprocessing), and knowledge of the physics of the underlying

357

phenomena incorporated into the model.



358

359 **Figure 6.** Scheme describing the operating mode of the direct problem (blue arrows) and

360 inverse problem (red arrows) methods for the case of the SIDRA-RU model

361 In the ‘forward’ or ‘simulation’ mode, the forcing terms (rainfall and PET) and the SIDRA-  
 362 RU model parameters are provided as known inputs in order to simulate the drainage  
 363 discharge. The ‘backward’ or ‘inverse’ mode seeks to estimate the unknown input parameters  
 364 by assimilating available information from the observed output discharge (Figure 6).

365 The recent paper written by Jeantet et al. (2021) presents an example that uses the “Michel  
 366 calibration (PAP-GR)” algorithm to estimate the parameters ( $K_{sat}$ ,  $\mu$ , SSDI and  $S_{inter}$ ). This  
 367 algorithm was originally developed at INRAE (formerly IRSTEA) to calibrate the GR (*Génie*  
 368 *Rural*) hydrological models (Perrin et al., 2003). An operational version of the algorithm  
 369 (*airGR*) is available in an R package (Coron et al., 2017). This method is initially based on  
 370 assigning a probability distribution law for each calibrated parameter in order to target the  
 371 optimal variation domain. The calibration procedure is then refined by searching for the  
 372 optimal parameter values within the pre-selected bounds. The objective function used through

373 the PAP-GR routine depends on the calibration target (e.g. low or high flow, volume  
 374 improvement). For more detail, one can refer to the paper of (Jeantet et al., 2021).

375 The VDA yields optimal estimates of the unknown parameters by minimizing the cost  
 376 function

$$377 \quad J(U) = \frac{1}{2} \|(R^{-1/2}M(U) - X^*)\|^2 + \frac{1}{2} \|B^{-1/2}(U - U_b)\|^2 \quad (12)$$

378 Under the box constraints  $a \leq U \leq b$ . Here,  $B = E(\xi_b \xi_b^T)$  and  $R = E(\xi_o \xi_o^T)$  are the  
 379 covariance matrices of the background and observation errors,  $\xi_b$  and  $\xi_o$ , respectively. As in  
 380 Section 2.3.1, we consider  $B = \text{diag}(\sigma_i^2), i = 1, \dots, \bar{n}$ , where  $\sigma_i$  is the standard deviation, and  
 381  $\bar{n}$  is the dimension of the control subset. Note that a-priori information on the parameters is  
 382 represented by the bounds  $a$  and  $b$ . Since (12) implies the Gaussian distribution of  $\xi_b$ , we  
 383 define  $\sigma_i = ((b_i - a_i)/2)/3$ .

384 The observation error  $\xi_o$  includes directly the measurement error, plus projections into the  
 385 observation space of other errors (forcing data errors, structural errors). Since  $R$  is difficult to  
 386 evaluate, we assume it is diagonal, with uniform variance  $\alpha^2$ . Then (12) can be written in the  
 387 form

$$388 \quad J(U, \alpha) = \frac{1}{2} \|(M(U) - X^*)\|^2 + \frac{\alpha^2}{2} \|B^{-1/2}(U - U_b)\|^2 \quad (12a)$$

389 Where  $\alpha$  has to be estimated alongside  $U$  from an auxiliary condition on  $U$ . This is a ‘relaxed’  
 390 formulation which roughly takes into account all uncertainties not included into the control  
 391 vector. In practice, instead of solving this problem explicitly, one can consider the  
 392 minimization problem for the cost function

$$393 \quad J(W) = \frac{1}{2} \|(M(U_b + B^{1/2}W) - X^*)\|^2 \quad (13)$$

394 Where  $W$  is defined via the change of variables  $U = U_b + B^{1/2}W$ , complemented with an  
395 appropriate iterations stopping criteria (L-curve). This is an iterative regularization  
396 implementation of (12a), as described in (Gejadze and Malaterre, 2017; Oubanas et al.,  
397 2018).

398 In the present study, a limited memory L-BFGS-B algorithm (Zhu et al., 1997) has been  
399 employed to perform the minimization step involving box-constrained set of parameters in  
400 order to avoid unphysical solutions. As explained above, the choice of the VDA method is  
401 largely motivated by the need to investigate and optimize the upgraded version of SIDRA-  
402 RU (to be reported in a future paper), which will be able to simulate the daily nitrate  
403 concentration values by integrating the unknown distributed variable, in addition to the model  
404 input parameters. The mentioned distributed variable represents the potentially leachable  
405 quantity of the nitrate initially trapped in the soil surface layer. This quantity is estimated  
406 once a year, generally at the end of the autumn season. The control vector will then be  
407 extended accordingly. For this reason, the choice of variational DA is justified since the  
408 algorithm sought needs to be robust to the present uncertainties and heterogeneity of the  
409 variables involved. Hence, this paper offers the first implementation of the VDA to SIDRA-  
410 type models, which will be adapted to the new upgraded version.

411 Let us note that (12) is the strong-constraint variational formulation, which is valid under the  
412 perfect model assumption. In the variational DA framework, the model error is usually  
413 treated via the weak-constraint formulation (Tremolet, 2006). This approach is proved useful  
414 in the classical DA in weather and ocean prediction systems, where the model state at the  
415 beginning of the prediction window is of major concern. In hydrology, the method has been  
416 used as a part of the hybrid-filtering algorithm in (Abbaszadeh et al., 2019). However, the  
417 usefulness of the weak formulation for solving the pure calibration problems is far less  
418 evident. Besides, being a conceptual and approximate model, SIDRA-RU is characterized by

419 a structural uncertainty, which is not exactly the model error as it is understood in the  
420 classical applications (for example, due to random forcing). A more appropriate approach to  
421 deal with the structural uncertainty seems the model selection in the Expectation-  
422 Maximization framework (Beal, 2003). This is a topic for a possible future development, but  
423 we keep the strong-constraint DA formulation as a first step in this direction.

#### 424 ***2.4.1. Toward avoiding the local minima issues***

425 Due to the ill-posedness of certain inverse problems, the corresponding minimization process  
426 may suffer from the presence of the local minima, which prevent it from reaching the global  
427 one. Various approaches have been investigated to mitigate this difficulty. Inspired by the  
428 works of Duan et al. (1992) and Skahill and Doherty (2006), we suggest using an ensemble  
429 minimization framework. The idea here is to start each individual minimization process from  
430 a different first guess, which might result in different minimization trajectories, thus limiting  
431 the dependence of the optimal solution from the prior knowledge and its uncertainty. The  
432 ensemble of priors/backgrounds (used as initial points for minimization) is generated using a  
433 uniform distribution and is limited to the sufficient subset elements, as identified through the  
434 GASA method (see Section 3.1). Two configurations have been tested herein: 1) the input  
435 parameters are perturbed one by one, setting the remaining ones at their optimal values; and  
436 2) parameters are perturbed simultaneously. The ensemble size is then chosen to compromise  
437 target accuracy and available computational resources.

#### 438 ***2.4.2. Hybrid BV method: description***

439 As mentioned above, if the estimation problem is ill-posed in terms of the uniqueness  
440 condition, looking for the global minimum might be useless in principle. That is, the resulting  
441 posterior distribution could be multi-modal, with modes having nearly the same probability  
442 values, but corresponding to noticeably different combinations of parameters. Since both the

443 model and the observations are not 'perfect', choosing the posterior mode with the largest  
 444 probability (or the 'global' minimum in terms of the cost-function) could be a wrong  
 445 decision. Thus, the remedy is to look for the posterior mean instead. This should result into  
 446 more robust (reliable) parameter estimates. Since the direct use of the Bayesian methods  
 447 could be computationally too expensive, we suggest a novel hybrid BV method combining  
 448 variational and Bayesian elements, which can be considered as an upgrade to the method  
 449 presented in (Skahill and Doherty, 2006).

450 Let us consider an ensemble of optimal solutions  $U_i, i = 1, \dots, N$ , where each  $U_i$  is the result  
 451 of minimization of the cost-function (13), involving a randomly chosen background  $U_b$  from  
 452 the probability distribution  $\rho(U)$ . Let  $J_i = J(U_i)$  be the corresponding value of (13), and  $J_{min}$  –  
 453 the minimum value of  $J_i$  over the ensemble. Now we introduce the likelihood function in the  
 454 form:

$$455 \quad \mathcal{L}_i^k = \exp\left(-2^k \left(\frac{J_i}{J_{min}} - 1\right)^2\right) \quad (14)$$

456 where  $k$  is the parameter, which controls the decay rate of the likelihood function. This  
 457 parameter is similar to the regularization parameter used in the classical Tikhonov approach.  
 458 Then, the posterior ensemble mean and variance are computed as follows:

$$459 \quad \bar{U}^k = \frac{1}{c_1} \sum_{i=1}^N U_i \mathcal{L}_i^k \rho(U_i) \quad (15)$$

$$460 \quad Var(U)^k = \frac{1}{c_1} \sum_{i=1}^N (U_i - \bar{U}^k) \circ (U_i - \bar{U}^k) \mathcal{L}_i^k \rho(U_i) \quad (16)$$

461 where 
$$c_1 = \frac{1}{N} \sum_{i=1}^N \mathcal{L}_i^k \rho(U_i)$$

462 The L-curve approach is adapted here for choosing  $k$ . L-curve is defined as a parametric  
 463 curve  $\{J(\bar{U}^k), D^k\}, k = -20, \dots, 20$ , where

$$464 \quad D^k = (\bar{U}^k - \bar{U}^{-\infty})^T (Var(U)^k)^{-1} \circ (\bar{U}^k - \bar{U}^{-\infty}) \quad (17)$$

465 is the probabilistic (Mahalanobis) distance between  $\bar{U}^k$  and

$$466 \quad \bar{U}^{-\infty} = \frac{1}{N} \sum_{n=1}^N U_n \quad (18)$$

467 The idea of the ‘L-curve’ method is to choose the value of  $k$  located near the corner, so that  
468 both the cost-function  $J(\bar{U}^k)$  and the distance  $D^k$  are simultaneously minimized. One  
469 particular example of the L-curve encountered during computations is presented in Figure 13.  
470 Note that the uniform prior distribution for  $U_b$  is assumed in this paper, therefore the  
471 posterior moments are fully defined by the likelihood function (14).

## 472 **2.5. Evaluation of the temporal robustness of the model**

473 An ensemble of operational tests proposed by Klemeš (1986) has been widely used to  
474 evaluate the spatiotemporal robustness of hydrological models (Henriksen et al., 2003; Guo et  
475 al., 2020; Jeantet et al., 2021). In the following, we have selected the split sample test to  
476 evaluate the temporal robustness of the SIDRA-RU model. This method divides the study  
477 period into two subperiods (e.g.  $P_1$  and  $P_2$ ). The first window  $P_1$  is considered as an  
478 assimilation period. Hence, the daily discharge is assimilated using VDA in order to estimate  
479 the control vector  $U$ . The parameter estimates obtained are then validated by comparing the  
480 corresponding model predictions with observations over the period  $P_2$ . Next, the assimilation  
481 and validation periods  $P_1$  and  $P_2$  are swapped to validate the estimator’s temporal robustness.

482 Overall, four metrics have been selected to evaluate the model's predictive performance. One  
483 can recall the cost function (Section 2.4; Equation 13) and the KGE metric (Section 2.3.1;  
484 Equation 7), relevant to assess the variability of the drainage discharge. In addition, we use  
485 the root mean square error (RMSE (Kenney, 1939)), which informs of the residuals spread.

$$486 \quad RMSE = \sqrt{\frac{\sum_{i=1}^N (X_i^* - X_i)^2}{N}} \quad (19)$$

487 and the Nash-Sutcliffe Efficiency (NSE (Nash and Sutcliffe, 1970)), as defined in Equation  
488 20, which is introduced to assess the performance of several hydrological and water quality  
489 models.

$$490 \quad NSE = 1 - \frac{\sum_{i=1}^N (X_i^* - X_i)^2}{\sum_{i=1}^N (X_i - \bar{X}^*)^2} \quad (20)$$

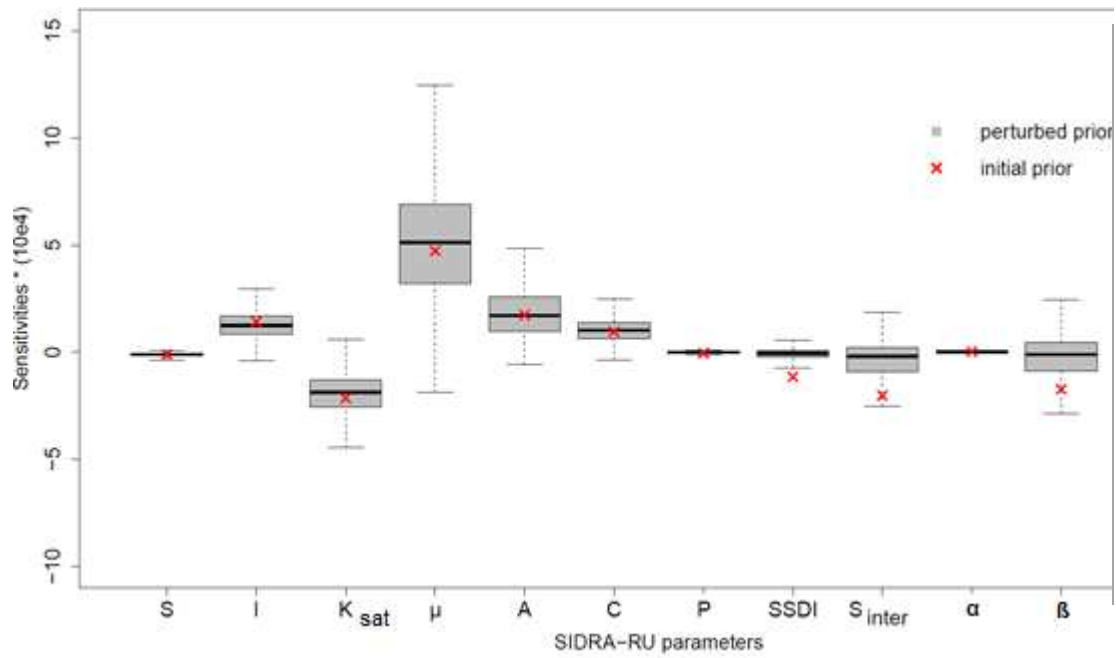
491 In addition, we are quantifying the water balance conservation by calculating the discrepancy  
492 on cumulative drained water volumes.

### 493 **3. RESULTS**

#### 494 **3.1. Adjoint local and global sensitivity analyses**

495 The LASA method was first applied to assess the influence of SIDRA-RU input parameters  
496 on the KGE metric. First, the local sensitivity around 'pre-calibrated prior' (Table 2) was  
497 computed (as illustrated in Figure 7 with red crosses) using the entire data (Figure 3). Results  
498 show that the highest sensitivities are to soil parameters  $\mu$  and  $K_{sat}$  and reservoir parameter  
499  $S_{inter}$ .

500 Second, in order to investigate the impact of the prior on the resulting sensitivities, a set of  
501 1000 random input values has been generated using the uniform distribution defined over the  
502 interval [a,b] (Equation 8 and Table 2). The corresponding sensitivities have been then  
503 computed using LASA. The boxplots in Figure 7 show the range of impact of each  
504 parameter. The highest range is observed for parameters  $K_{sat}$ ,  $\mu$  and further  $S_{inter}$   $A$  and  $\beta$   
505 whereas the smallest range was identified for parameters  $S$ ,  $P$  and  $\alpha$ .



506

507 **Figure 7.** Sensitivities of the “KGE metric” using a single 'pre-calibrated prior', in red  
 508 crosses; using ensemble of priors, in boxplots

509 Further analysis has therefore been performed using the GASA method over the entire range  
 510 of parameter variation, as defined within bounds [a,b]. A random ensemble of SIDRA-RU  
 511 input parameters has been generated from the uniform distribution. The ensemble size was  
 512 chosen to balance the stability of results and low CPU time. Hence, testing different ensemble  
 513 sizes (ranging from 100 to 10000) allowed the selection of  $n = 2000$ , ensuring stable  
 514 sensitivity results. One can note that only  $\sim 2.6$  s was needed to complete the 2000  
 515 simulations.

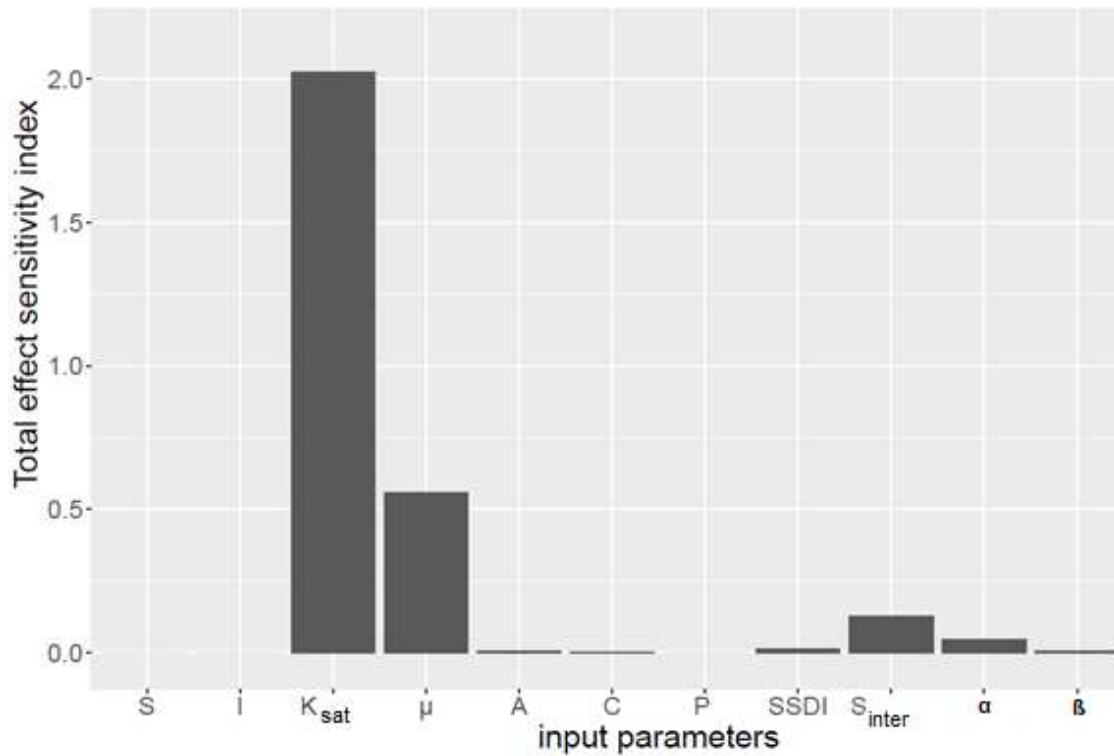
516 Table 2 lists the values of the boundaries (a) and (b) assigned according to both the prior  
 517 knowledge of SIDRA-RU model parameters and the data collected from the Chantemerle  
 518 field. Accordingly,  $K_{sat}$ ,  $\mu$ ,  $S_{inter}$ , and  $SSDI$  parameter bounds have been selected from  
 519 (Henine et al., 2022). The other parameter boundaries was assigned so as to avoid outliers.

520

**Table 2.** Minimum (a) and maximum (b) values defined for each parameter

<b>Input</b>	<b>S</b> <b>(ha)</b>	<b>I</b> <b>(m)</b>	<b>K<sub>sat</sub></b> <b>(m/day)</b>	<b>μ</b> <b>(-)</b>	<b>A</b> <b>(-)</b>	<b>C</b> <b>(-)</b>	<b>P</b> <b>(m)</b>	<b>SSDI</b> <b>(mm)</b>	<b>S<sub>inter</sub></b> <b>(mm)</b>	<b>α</b> <b>(-)</b>	<b>β</b> <b>(-)</b>
<b>a</b>	35.40	3.50	0.02	0.010	0.80	0.85	0.60	10.00	55.00	0.00	0.50
<b>b</b>	37.40	6.00	1.00	0.130	0.90	0.95	1.20	55.00	225.00	1.00	1.00
<b>Pre-calibrated Prior</b>	36.40	5.00	0.27	0.042	0.86	0.89	0.90	46.48	92.58	0.33	0.90

521 The obtained ‘total-effect’ sensitivities using the GASA approach are shown in Figure 8. The  
522 results indicate that the saturated hydraulic conductivity  $K_{sat}$  is the most influential input  
523 parameter, followed by the drainage porosity  $\mu$  and then the intermediate water level  
524 threshold in the conceptual reservoir  $S_{inter}$ , followed by the other parameters. This finding  
525 means that only  $K_{sat}$ ,  $\mu$  and subsequent  $S_{inter}$  parameters exert the strongest impact on KGE  
526 values. Although  $SSDI$  is classified as a low-impact parameter, it is included in the control  
527 vector due to its strong link with  $S_{inter}$  parameter (Section 2.2).



528

529

**Figure 8.** The influence of input parameters on the valuable function J (KGE)

530

### 3.2. SIDRA-RU parameters estimation using the VDA method

531

Based on the results of GASA (Section 3.1), the VDA method was implemented to estimate

532

the impacting part of the input vector on the model output (i.e.  $U = \{K_{sat}, \mu, S_{inter}, SSDI\}$ ).

533

Two experimental set-ups have been considered:

534

a) the split sample test, considering the two-time windows  $P_1$ , covering the period from

535

2008 to 2010, and  $P_2$  covering the period 2010-2013, to assess the model's predictive

536

performance;

537

b) the full sample test (over the entire observation period,  $P_1 \cup P_2$ ), with the resulting

538

simulated discharge to be compared to the one obtained with parameters estimated

539

using the PAP-GR calibration method.

540 **3.2.1. Validation of the variational DA framework**

541 Table 3 shows the results of the split sample test. Good performance in terms of KGE, NSE  
 542 and RMSE is achieved for both the assimilation and validation periods (KGE > 0.66; NSE >  
 543 0.53; RMSE < 2.44 l/s). Moreover, swapping the assimilation and validation periods  $P_1$  and  
 544  $P_2$  leads to relatively comparable estimates (e.g.  $S_{inter}$  estimated at 71.2 mm and 85.8 mm  
 545 over periods  $P_1$  and  $P_2$ , respectively), and similar performance metric values. One can also  
 546 notice that distances between the SIDRA parameters (e.g.  $\mu$  on  $P_1$  vs  $\mu$  on  $P_2$ ) are smaller  
 547 compared to those for the conceptual parameters (e.g.  $S_{inter}$  on  $P_1$  vs  $S_{inter}$  on  $P_2$ ).

548 **Table 3.** Split sample test results based on assimilation of the drainage discharge data

Simulations	Estimation period				Validation period				Estimated parameters			
	P1 (2008-2010)				P2 (2010-2013)							
	RMSE	NSE	KGE	Cost	RMSE	NSE	KGE	Cost	$K_{sat}$	$\mu$	SSDI	$S_{inter}$
	(l/s)	(-)	(-)	(-)	(l/s)	(-)	(-)	(-)	(m/d)	(-)	(mm)	(mm)
P1 → P2	1.62	0.56	0.66	0.74	2.44	0.71	0.77	2.50	0.19	0.042	40.8	71.2
	Validation period				Estimation period				Estimated parameters			
	P1 (2008-2010)				P2 (2010-2013)							
P2 → P1	1.66	0.53	0.70	0.78	2.41	0.72	0.77	2.45	0.23	0.042	35.2	85.8

549 **3.2.2. VDA vs. Gradient-free PAP-GR method**

550 Below, the VDA method is compared to the gradient-free PAP-GR calibration method by  
 551 estimating the control vector values over the entire observation period (2008-2013). Three  
 552 experimental configurations are considered with the following sets of input parameters:

- 553 • (a) Non-informative (open-loop) inputs (priors/backgrounds)
- 554 • (b) Calibrated inputs from Michel’s calibration algorithm (PAP-GR)
- 555 • (c) Estimated inputs from the VDA method, taking the background values from (a)

556 Table 4 shows the input parameters obtained for configurations (a), (b) and (c), along with  
 557 the corresponding performance metrics values. Note that the improvement achieved by VDA  
 558 compared to the PAP-GR calibration algorithm is indicated in green brackets.

559 **Table 4.** Performance criteria resulting from: (a) the use of open-loop parameters; the  
 560 parameter estimation using both (b) the PAP-GR and (c) the VDA minimization methods

	Control vector values				Performance criteria		
	$K_{sat}$ (m/day)	$\mu$ (-)	SSDI (mm)	$S_{inter}$ (mm)	RMSE (l/s)	NSE (-)	KGE (-)
<b>a</b>	0.9	0.06	18.0	30.0	4.66	-0.46	0.08
<b>b</b>	0.272	0.043	46.48	92.58	2.13	0.70	0.76
<b>c</b>	0.228	0.044	41.93	84.84	2.07 (-0.06)	0.71 (+0.01)	0.78 (+0.02)

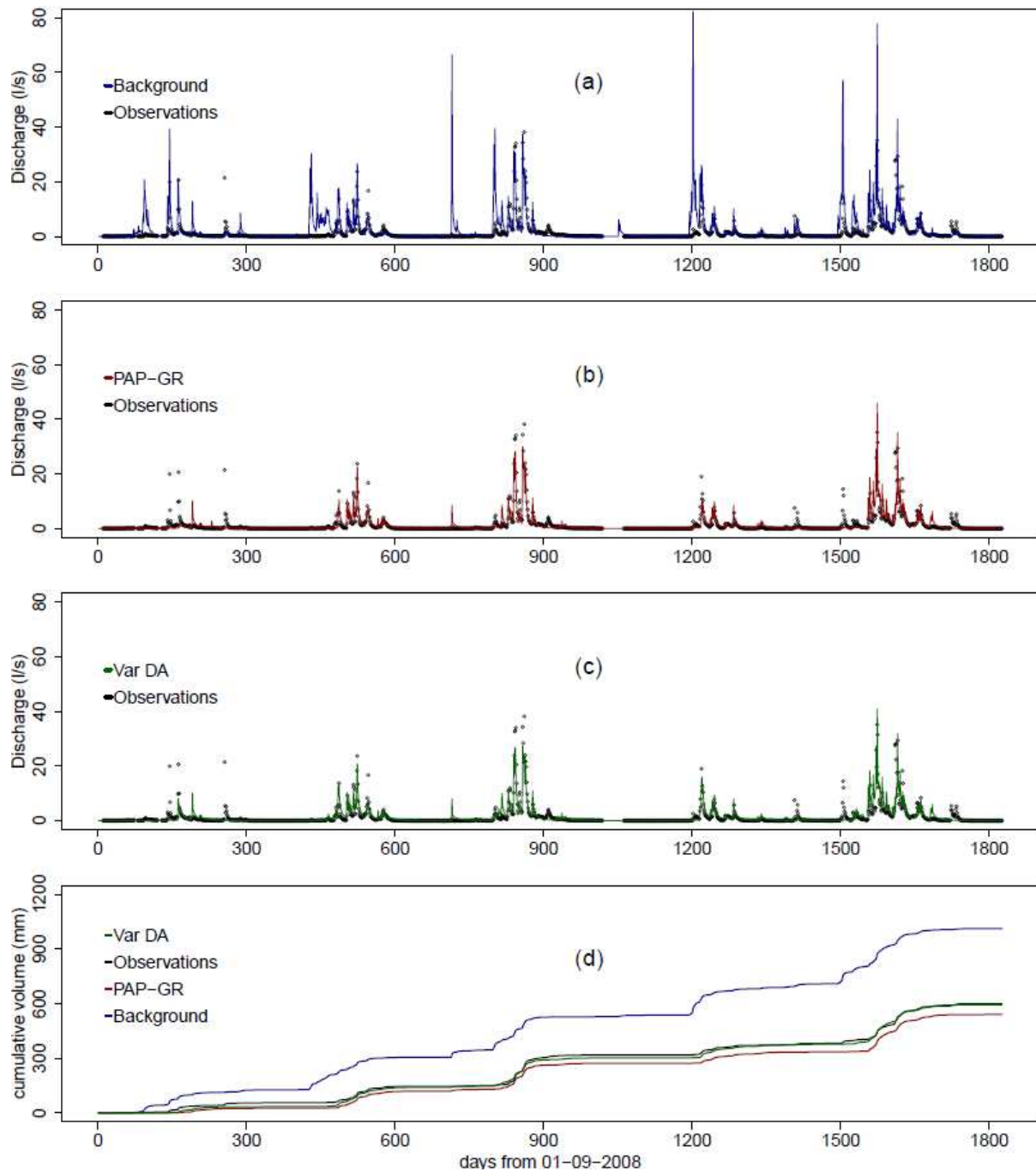
561 In the experimental set-up (c), the VDA is used starting from a non-informative background  
 562 from (a) in order to estimate input parameters  $K_{sat}$ ,  $\mu$ ,  $S_{inter}$  and  $SSDI$  simultaneously. Since  
 563 the bounds of the physical parameters range have not been integrated into SIDRA-RU, a  
 564 constrained cost minimization is performed using the L-BFGS-B method to eliminate all non-  
 565 physical solutions. Table 5 summarizes the lower and upper bounds assigned to each  
 566 parameter. The choice of  $K_{sat}$  and  $\mu$  bounds is based on field measurements carried out in 70  
 567 referenced soils in France (Lagacherie, 1987).  $SSDI$  and  $S_{inter}$  bounds are presented in  
 568 (Henine et al., 2022). The estimated control vector (c) is comparable to that derived from the  
 569 split sample test in the first experiment (Table 3).

570 **Table 5.** Assigned lower and upper bound values of each calibrated input parameter

Parameter	$K_{sat}$ (m/day)	$\mu$ (-)	SSDI (mm)	$S_{inter}$ (mm)
Lower bound	0.03	0.02	10.0	55.0
Upper bound	1.5	0.07	60.0	225.0

571 Figure 9 illustrates the observed and simulated discharges, over the total target period,  
572 according to the three experimental configurations (a, b, c). In addition, the respective  
573 cumulative water volume has been plotted in (d), thus making it possible to compare the  
574 performance obtained using the variational calibration method and that resulting from the  
575 application of the PAP-GR calibration algorithm.

576 The model performance after VDA is slightly better in terms of KGE, NSE and RMSE  
577 values, as compared to the PAP-GR calibration routine. Excluding the first year of data,  
578 generally used as a warming period to adjust the saturation degree in the conceptual reservoir,  
579 the discharge values are well represented in both cases (Figure 9b and 9c). In addition, the  
580 analysis of the simulated cumulative drained water over the total target period (five drainage  
581 seasons) in comparison with the measured discharge, indicates only a 1% ratio between  
582 measured and simulated total drained water volume using VDA ( $\Delta V = 4.8$  mm over five  
583 years of data; Figure 9d) versus 10% when using the PAP-GR calibration algorithm ( $\Delta V =$   
584 58.7 mm).



585

586 **Figure 9.** Graphical comparison between experimental configurations (a), (b) and (c);

587 (d) shows the corresponding cumulative drainage discharge

### 588 3.3. Investigating the local minima issue

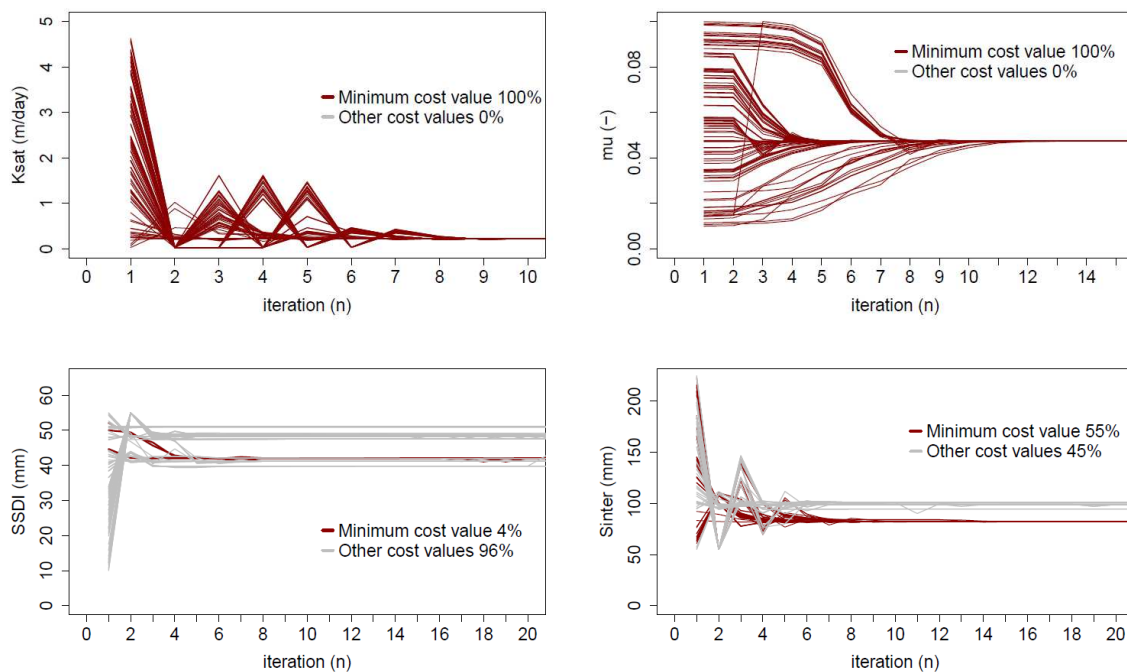
589 The second part of this study focuses on the issue of local minima. Two experimental set-ups

590 have been considered. First, we analyze the convergence process for a given single

591 parameter, assuming that the remaining parameters are known and set to their optimal values.  
 592 Second, we investigate the convergence process when all parameters are updated  
 593 simultaneously.

### 594 3.3.1. Single parameter estimation

595 In this experiment, each parameter  $U_i$  is estimated separately while assuming that all other  
 596 inputs are known and set to their optimal values (Table 4, Row C). Hence, the control vector  
 597 includes one parameter at a time. For each parameter  $U_i$ , an ensemble of priors/backgrounds  
 598 of size  $n=100$  is generated and an ensemble estimation using the VDA is performed. Figure  
 599 10 illustrates the convergence process for each parameter, starting from different initial  
 600 values within the given ensemble. The red color represents successful minimization cases,  
 601 where a cost function minimization has been reached. The corresponding ratios are presented  
 602 in the legend, together with the unsuccessful cases shown in gray. Note that minimum cost  
 603 values are generally reached after only 10 iterations.



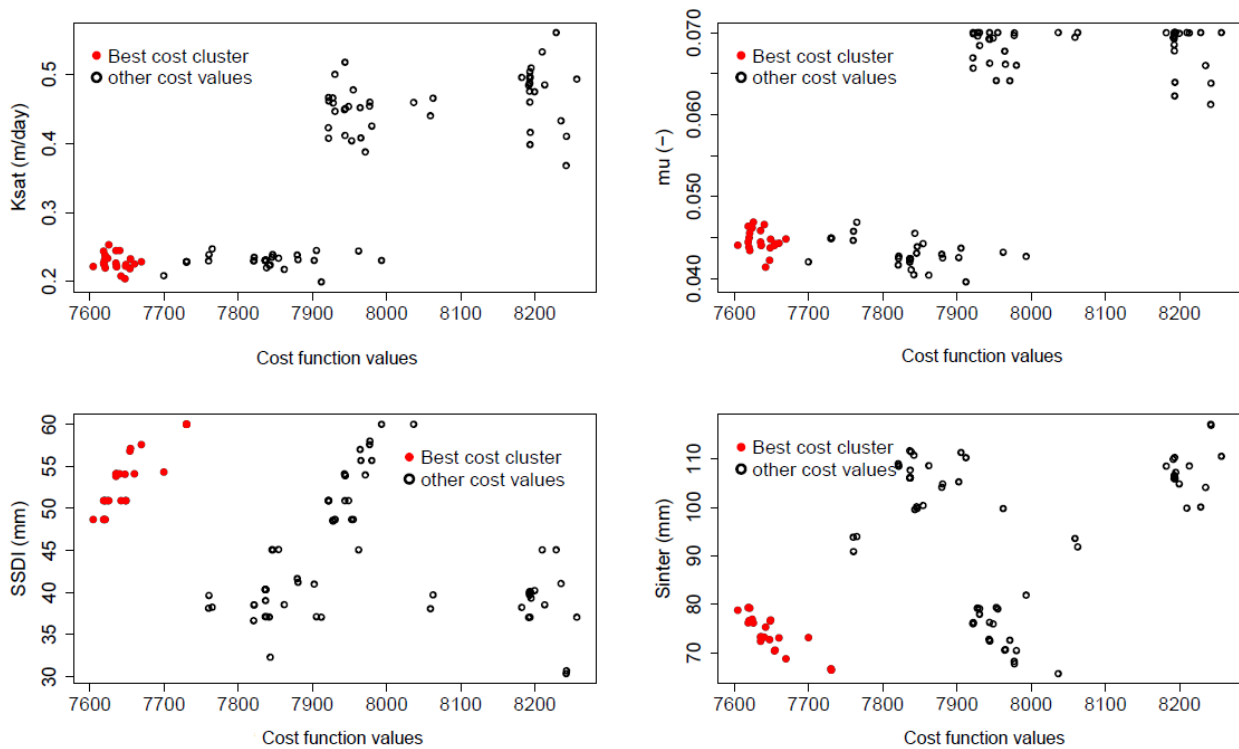
604

605 **Figure 10.** Convergence trajectories of parameters from prior/background values towards the  
 606 optimal values during the single parameter estimation process

607 It can be noticed that the ensembles of parameters  $K_{sat}$  and  $\mu$  converge towards unique  
 608 values of 0.22 m.d<sup>-1</sup> and 0.047, respectively, regardless of the initial background value.  
 609 However,  $SSDI$  and  $S_{inter}$  parameters converge towards different optimal values. Those  
 610 corresponding to the minimum cost function are 42 mm and 82 mm, respectively, which are  
 611 still consistent with the result obtained in Section 3.2.

### 612 3.3.2. Simultaneous minimization

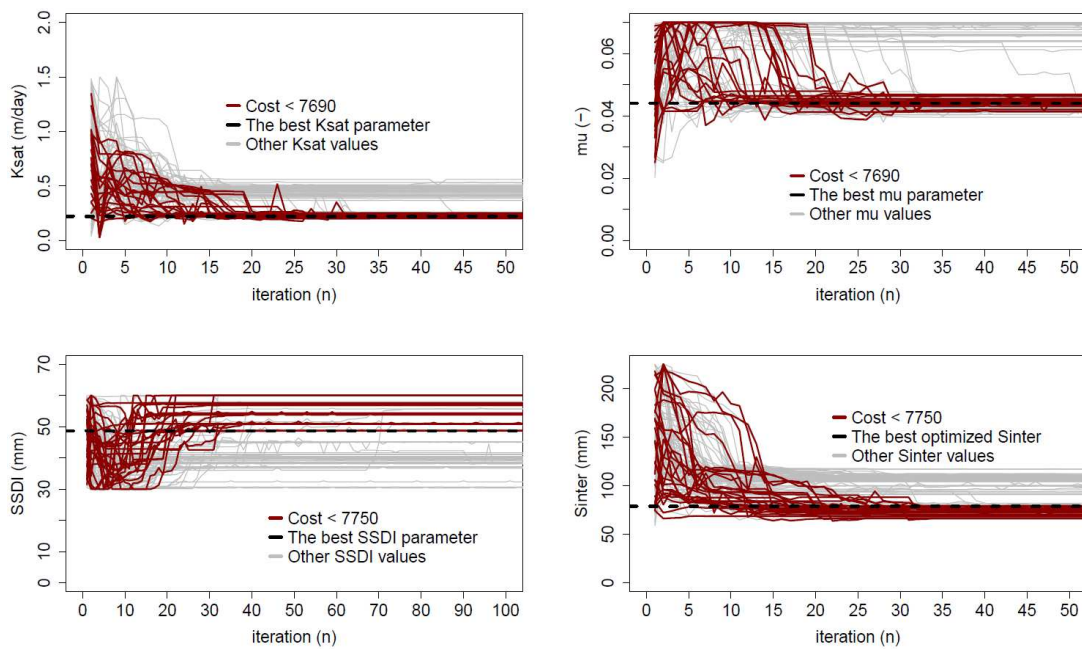
613 Similar to the first set-up, in this second experiment, an ensemble of size n=100 of  
 614 prior/background vectors is generated. The simultaneous minimization of all parameters was  
 615 then performed using the VDA method. Figure 11 shows the parameter sets that converge  
 616 toward minimum cost function values, presented here in red. Four main clusters (red dots)  
 617 have been identified. Similar cluster positions for the two physically based parameters  $K_{sat}$   
 618 [0.19-0.25] m.d<sup>-1</sup> and  $\mu$  [0.040-0.047] can be detected. Interestingly, the conceptual-based  
 619 parameters  $SSDI$  [47-61] mm and  $S_{inter}$  [65-81] mm display opposite cluster positions.



620

621 **Figure 11.** Final cost values according to their corresponding parameter values

622 Similar to the first experiment, Figure 12 shows the minimization trajectories. The red color  
 623 refers to the successful convergence cases reaching the minimum cost function value. It can  
 624 be observed that several solutions are possible when estimating all parameters and no global  
 625 minimum can be clearly identified. Dashed lines correspond to the optimal solution of each  
 626 parameter in terms of the minimized cost function. The best control vector estimates  
 627 corresponds to:  $K_{sat} = 0.22$  m/day,  $\mu = 0.044$  (-),  $SSDI = 48.68$  mm, and  $S_{inter} = 78.76$  mm.



628

629 **Figure 12.** Convergence trajectories from prior/background values towards optimal values  
 630 (case of simultaneous minimization)

### 631 3.4. Hybrid BV approach to improve the solution stability

632 The model parameters are estimated by the hybrid BV method following the “split sample  
 633 test” methodology (see Section 2.5).

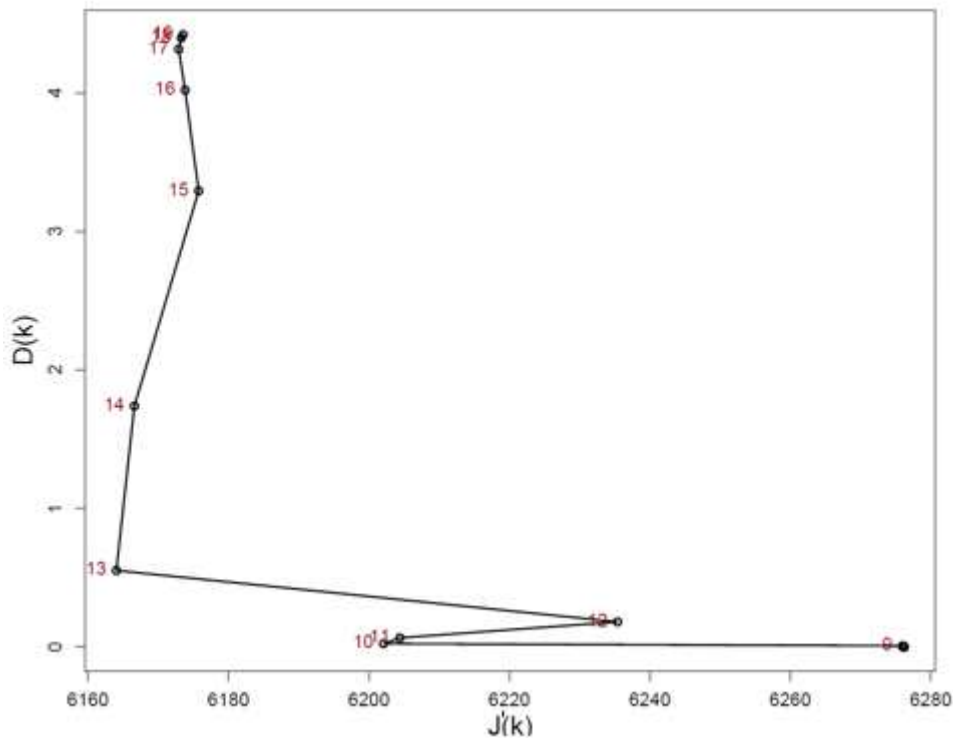
634 The parameter estimations presented in Table 3 (for P1 and P2), and Table 4 (for P) have  
 635 been embedded in Table 6 to allow a better comparison between hybrid DA and variational  
 636 DA methods. First, one can notice that the difference between the estimates  $K_{sat}$  and  $S_{inter}$   
 637 obtained using the hybrid DA on different periods P1 and P2 is less, whereas for  $\mu$  and  $SSDI$

638 is slightly larger. One key model characteristic which defines the water table dynamics is  
639 given by  $S_{max} = SSDI + S_{inter}$ . The difference  $S_{max|P2} - S_{max|P1}$  by the hybrid BV method  
640 makes 5.29 mm, against 9.1 mm by the variational DA. This indicates that the results by the  
641 hybrid BV method, as expected, are generally more robust. Secondly, while the estimates  
642  $K_{sat|P}$  and  $\mu|P$  are nearly the same for both methods, they are slightly different for  $SSDI|P$  and  
643  $S_{inter|P}$ .

644 **Table 6:** Robust SIDRA-RU parameter estimations obtained by applying both, Hybrid BV  
645 and VDA methods

Method	Parameter	$K_{sat}$ (mm.day <sup>-1</sup> )	$\mu$ (-)	SSDI (mm)	$S_{inter}$ (mm)	$S_{max}$ (mm)	k
Hybrid BV	Period P1 (2008-2010)	0.252	0.049	40.74	71.52	112.26	10
	Period P2 (2010-2013)	0.225	0.043	34.01	83.54	117.55	13
	Full period (2008-2013)	0.227	0.045	50.86	76.67	127.53	15
VDA	Period P1 (2008-2010)	0.190	0.042	40.80	71.20	112.00	-
	Period P2 (2010-2013)	0.230	0.042	35.20	85.80	121.00	-
	Full period (2008-2013)	0.228	0.044	41.93	84.84	126.77	-

646 As an example, Figure 13 shows the L-curve obtained by processing the ensemble of optimal  
647 solutions corresponding to P2 period. Here, one can see a distinctive corner at  $k = 13$ . This  
648 position ensures the robustness of the solution by selecting low values of  $D(k)$  and  $J(k)$ .



649

650 **Figure 13.** L-curve, Chantemerle P2 2010-13, “k” are plotted in dark-red color

#### 651 4. DISCUSSION

652 The paper’s content revolves around improving the new agricultural drainage model. First,  
 653 the adjoint sensitivity analysis (local and global) has been conducted to identify the most  
 654 impacting parameters of the SIDRA-RU model. Then, VDA and hybrid BV frameworks have  
 655 been validated over five years of daily-observed discharge data and used afterwards to  
 656 estimate the best combination of SIDRA-RU parameters.

#### 657 4.1. Adjoint SA

658 The local adjoint SA result suggests that  $\mu$  and  $K_{sat}$  are the most influential parameters.  
 659 However, one can notice that the choice of prior could change the parameter ranking which  
 660 emphasizes the importance of the global analysis. In fact, no priors are required to apply the  
 661 global adjoint approach. The global SA method indicates that  $K_{sat}$  and  $\mu$  have the most impact

662 on the model output. These two parameters govern the physically based part of the model and  
663 describe the dynamics and reactivity of the perched water table and discharges. The  
664 conceptual parameter  $S_{inter}$ , ranked third, controls the beginning of the intensive drainage  
665 season, which generally occurs during winter, while  $\beta$  is dependent on the type of vegetation  
666 cover. Since information on crop rotation is not always available, parameter  $\beta$  is set by  
667 default equal to 1. Future work will investigate the possibilities of integrating a crop rotation  
668 module should data be available.

669 The results obtained are consistent with the analysis performed using Sobol's total and main-  
670 order sensitivity indices in (Henine et al., 2022). This output confirms that  $K_{sat}$  and  $\mu$  have  
671 the highest impact on KGE, whereas  $SSDI$  and  $S_{inter}$  parameters practically determine the  
672 starting date of the drainage season. These four parameters constitute the sufficient control  
673 subset of parameters, or the 'control vector'. It should be noted that one limitation of the  
674 Sobol method is the significant computing resources required (Iooss and Lemaître, 2015;  
675 Zhang et al., 2015). This constraint accounts for the main reason why the analysis was  
676 conducted on a limited input vector in (Henine et al., 2022) paper. Such a limitation has been  
677 overcome by using the adjoint-based sensitivity analysis approach, which allows considering  
678 all SIDRA-RU inputs in a single model run. In addition, the limited number of SIDRA-RU  
679 input parameters avoids the need to use sophisticated sampling methods, e.g. Latin hypercube  
680 (Viana, 2016), which are typically reserved for models with higher number of inputs  
681 (Manache and Melching, 2004).

## 682 **4.2. Model parameters improvement**

683 The split sample test validates the accurate implementation of the VDA method. Moreover,  
684 we compare the estimated values of SIDRA-RU parameters with those found in the literature.  
685 Therefore, it has been possible to verify the estimated parameters against more than 100

686 reported values of  $K_{sat}$  and  $\mu$ , corresponding to the silty soil (consistent with the Chantemerle  
687 soil texture). The latter have been extracted by Jeantet et al. (2021) from the drainage  
688 reference sector reports (Lagacherie, 1987). The probability density functions (PDF) of the  
689 saturated hydraulic conductivity ( $K_{sat}$ ) and drainage porosity ( $\mu$ ) have been calculated using  
690 their lognormal distributions, with the most frequently observed values (modes)  
691 corresponding to 0.235 m.day<sup>-1</sup>, 0.017 for  $K_{sat}$  and  $\mu$ , respectively. The same soil texture  
692 could be found at the Arrou agricultural catchment (located 50 km south of Chartres, France),  
693 where the measured value of  $K_{sat}$  at subsoil depth equals 0.41 m.day<sup>-1</sup> (Zimmer et al., 1995).  
694 Therefore, the published data values of  $K_{sat}$  and  $\mu$  are close and consistent with the estimated  
695 values obtained by the VDA method.

696 Furthermore, Jamagne et al. (1977) and Goulet et al. (2004) sought to determine the water  
697 holding capacity (WHC) function of certain soil parameters (e.g. water content at field  
698 capacity and wilting point, apparent density). In these studies, the WHC ranged between 1  
699 mm.cm<sup>-1</sup> and 1.75 mm.cm<sup>-1</sup> for silty soil. Based on the drain depth of the Chantemerle field  
700 (90 cm), these values correspond to 90 mm and 157.5 mm, respectively. The estimates using  
701 VDA are therefore consistent with these values and lie within the WHC variation interval.  
702 The estimated SIDRA-RU parameters are listed in Table 7 alongside the field-scale observed  
703 data.

704 **Table 7.** Estimated SIDRA-RU parameters using VDA compared with those found in the  
705 literature

Source	$K_{sat}$ (m.day <sup>-1</sup> )	$\mu$ (-)	$S_{max}$ (mm)
Variational calibration	0.19; 0.23	0.044	112; 121
(Lagacherie, 1987)	0.235	0.017	-
(Bouarfa, 1995)	0.4	0.026	
(Zimmer et al., 1995)	0.41	-	-

Jamagne et al. (1977) & Goulet et al. (2004)	-	-	[90, 157]
---	---	---	-----------

706 One can see that VDA performs slightly better in terms of metrics evaluation (e.g. NSE,  
707 KGE) than the PAP-GR calibration. These results indicate that VDA could be seen as a  
708 relevant methodology to improve the predictive performance of the SIDRA-RU model. While  
709 the adjoint model of SIDRA-RU has been successfully obtained through the automatic  
710 differentiation (AD) tool TAPENADE, other large-scale models may need substantial  
711 programming effort and forward model adaptation to get the adjoint code. As an alternative,  
712 some methods, including the reduced adjoint approach, have been proposed to avoid  
713 laborious adjoint implementations (Antoulas, 2005; Altaf et al., 2013) but they require many  
714 function evaluations and converge towards approximate solutions (LeGresley and Alonso,  
715 2000). Overall, the task of generating the adjoint of any upgraded version of the conceptual  
716 SIDRA-RU model looks straightforward, given that certain coding rules are being respected.

### 717 **4.3. Water balance simulation**

718 A recent drainage modeling study, which aims to demonstrate the benefit of using a multi-  
719 objective minimization approach to improve the estimation of HYDRUS parameters, has  
720 shown a significant deviation (25%) between the cumulative measured and simulated water  
721 volumes, which corresponds to 50 mm in just one drainage season (Turunen et al., 2020). In  
722 this paper, a relevant result confirms the strong ability of VDA to simulate accurately the  
723 volume of water exported from drained agricultural fields. In fact, less than 1% ratio between  
724 measured and simulated total drained water volume is obtained using VDA ( $\Delta V = 4.8$  mm  
725 over five years of data, less than 1 mm/year). The robustness of the VDA method  
726 implemented with the SIDRA-RU model has been successfully validated in Section 3.2.1  
727 using the split sample test. It allows for a robust estimation of model parameters consistent  
728 with the *in-situ* values found in the literature. Moreover, the estimation of SIDRA-RU

729 parameters using VDA instead of the PAP-GR calibration approach improves the daily  
730 discharge simulations and the cumulative water volume predictions, in particular. Finally, it  
731 would be worthwhile to investigate the impact of the sampling interval on the water volume  
732 prediction by considering weekly or be-weekly discharge observations instead of daily ones  
733 (Oubanas et al., 2018).

#### 734 **4.4. Local minima issues**

735 Local minima issues is commonly encountered when solving ill-posed problems in  
736 variational formulations involving a gradient-based minimization. The application of  
737 sophisticated global optimization methods (e.g. Monte Carlo) could be useful to deal with  
738 strongly nonlinear systems (Hoteit, 2008). Here, we investigate a preliminary ensemble  
739 minimization framework, aiming to reach a stable global minima solution.

740 Consequently, the convergence of  $K_{sat}$  and  $\mu$  parameters towards a global minimum during  
741 the single optimization experiment highlights the strong consistency of the physically based  
742 SIDRA-RU module. However, the convergence pattern for parameters  $SSDI$  and  $S_{inter}$   
743 differs: dependent on the priors, the minimization process converges to different cost function  
744 values, which underscores the presence of local minima or equifinality issues. In fact, these  
745 two parameters manage the conceptual part of the SIDRA-RU model; their contribution is  
746 limited to a short period, essentially during the first few days of each drainage season. Our  
747 results suggest that their values may require a dynamic year update during the minimization  
748 process. Additional information on the reservoir capacity or beginning of the drainage season  
749 may be needed to constrain further the minimization protocol concerning these reservoir  
750 parameters.

751 It is worth noting that the convergence speed may depend on the modeling approach (e.g.  
752 conceptual or physical, distributed or not), the choice of the optimization algorithm, and the

753 parameter type. In fact, SIDRA module parameters (e.g.  $K_{sat}$ ,  $\mu$ ) find a stable solution  
754 following 20 iterations while conceptual ones (e.g.  $SSDI$ ,  $S_{inter}$ ) generally need 30 iterations.  
755 This explains the notable difference observed between the cost function thresholds.

756 Chossat and Saugnac (1985) highlight a potential relationship between  $K_{sat}$  and  $\mu$  for  
757 different soil textures. Our finding suggests that these two groups of parameters are  
758 complementary and may compensate each other, which typically leads to the occurrence of  
759 local minima and equifinality issues (nearly the same prediction obtained with different  
760 parameter values). The equifinality issue can be mitigated when assimilating additional  
761 information by the VDA, e.g. water level variations  $h(t)$ . We suggest herein that  
762 complementary information (namely nitrate concentrations  $[NO_3^-]$  and fluxes) will  
763 additionally constrain the solution in the upgraded SIDRA-RU version. The featured methods  
764 have been implemented in order to improve both the understanding and estimation of the  
765 SIDRA-RU input parameters. The present work can be extended to other drainage models.

#### 766 **4.5. The potential of the hybrid BV approach**

767 The implementation of the hybrid BV framework improves the stability of the obtained  
768 solution compared to the classical VDA. That is, the estimated parameters are more  
769 consistent from one study period to the other, which demonstrates the robustness of the  
770 proposed method. In fact, the estimated parameter values on P1 and P2 are similar (Table 6),  
771 in particular for the parameters  $K_{sat}$  and  $S_{max}$  (the reported difference between P1 and P2  
772 estimated values are  $0.027 \text{ mm.day}^{-1}$  and  $5.3 \text{ mm}$ , respectively). Moreover, the approach  
773 offers an automatic tool to select, cleverly and objectively, the most suitable and robust set of  
774 parameters, which was not the case by using visual interpretations (section 3.3). It is  
775 worthwhile in this context to discuss the results of the latest SIDRA-RU developments  
776 (Jeantet et al., 2021; Henine et al., 2022), which highlight the performance of the model in

777 terms of discharge simulations and the robustness of the estimated parameters. It was  
778 observed that conceptual based parameters (e.g.  $S_{\max} = \text{SSDI} + S_{\text{inter}}$ ) show a large deviation  
779 range [50 mm, 150 mm]. These estimated values remain scattered, regardless of their  
780 consistency as compared to the literature-based values (c.f. Table 7, last row). Otherwise, the  
781 limited number of information available in the literature makes complex any confrontation  
782 between the estimated conceptual parameters of the model and the field measurement values.  
783 Moreover, the structure of the conceptual block of the model may need some additional  
784 information to be able to manage the related parameters in a robust way and with a reduced  
785 level of uncertainty (e.g. hourly discharge observations, time-variant estimation of the  
786 conceptual parameters). In addition, let us note that any reliable conclusions on the relative  
787 performance of the two methods (hybrid BV against variational DA) cannot be made on a  
788 single test example, even within the identical twin experiment framework, where the 'true'  
789 values of parameters are known. This is significantly more difficult when considering  
790 realistic data and an approximate model (which is often the case with conceptual models).

## 791 **5. CONCLUSIONS**

792 Our first objective has been to evaluate the impact of the SIDRA-RU input parameters on the  
793 model output, to rank them and form a sufficient control set. This has been achieved using  
794 both local and global adjoint sensitivity analysis. Then, the parameters from the control set  
795 have been estimated by assimilating the drainage discharge data, collected from the 36-ha  
796 Chantemerle agricultural field for the period 2008-2013, using VDA.

797 In addition to the local adjoint SA, the global adjoint SA method has been investigated in  
798 application to the SIDRA-RU model. Based on estimating the upper bound of the "total-  
799 effect" Sobol indices, the GASA method has shown results consistent with the classical Sobol  
800 method (applied to the same model). In particular, the results of this analysis demonstrate that

801 the two most influential parameters are  $K_{sat}$  and  $\mu$ . The GASA method has proven to be  
802 capable of estimating the impact of all input parameters at a very low computational time ( $\approx$   
803 2.6 s). As a result, only 4 (out of 11) parameters have been selected for the calibration step.

804 The VDA method has been successfully implemented on the conceptual-analytical model  
805 SIDRA-RU. This method has been validated using the ‘split sample test’ and compared to  
806 Michel’s step-by-step calibration method (PAP-GR). Slightly better performance could be  
807 noted with the VDA method, which allowed estimating the best parameter set and  
808 reproducing a satisfactory daily drainage discharge simulation (KGE = 0.76 for PAP-GR vs.  
809 0.78 for VDA). An important advantage of these estimates has been revealed by comparing  
810 the total cumulative drainage volumes. The parameters estimated using the VDA method  
811 yielded a cumulative volume close to the observed volume at the field outlet (not exceeding  
812 4.8 mm and less than 1% discrepancy) compared to values obtained with PAP-GR (58.7 mm,  
813 for a 10% error). Moreover, the corresponding parameter values are consistent with those  
814 found in the literature under similar soil conditions (i.e. texture, climate). A planned  
815 forthcoming work will be to assimilate the nitrate concentration observations using the  
816 upgraded version of SIDRA-RU, which will integrate a newly developed nitrate transport  
817 model. We expect that the advantages of the implemented approach will be particularly  
818 beneficial for the coupled drainage/nitrate model, since it requires yearly estimations of a  
819 given input variable.

820 Lastly, the local minima issue has been explored. Our results here are in line with findings  
821 reported in the literature. It has been confirmed that using gradient-based minimization may  
822 lead to multiple possible solutions due to local minima. Therefore, a novel hybrid BV method  
823 has been implemented. Starting from an ensemble of optimal solutions given by VDA, the  
824 posterior PDF is computed using a specially defined likelihood function. At least, in theory,

825 the hybrid BV method has to provide a more robust estimate of the parameters (in average  
826 sense, i.e. over a representative set of the test cases). The fact that significantly different  
827 estimates for  $SSDI$  and  $S_{inter}$  have been obtained in the split sample test underlines the  
828 importance for further investigation in this direction.

## 829 **ACKNOWLEDGMENTS**

830 This research was supported by a PhD Grant from INRAE AQUA department. The authors  
831 would like to thank Irina Ginzburg for giving precious comments to improve this paper. We  
832 also thank farmers of the Chantemerle parcels and GIS ORACLE project for providing  
833 hydrological and climatic data.

## 834 **DATA AVAILABILITY**

835 Data archiving is underway. An upload within OZCAR network is scheduled (ORACLE  
836 <https://gisoracle.inrae.fr/>).

## 837 **REFERENCES**

- 838 Vincent, B., 2020. Principes techniques et chiffres du drainage agricole. De la tuyautique à  
839 l'hydro-diplomatie. Sciences Eaux Territoires(2): 8-15.
- 840 Mohtadullah, K., 1990. Interdisciplinary planning, data needs and evaluation for drainage  
841 projects, Land drainage - Drainage agricole : actes du 4ème séminaire international  
842 sur le drainage, Le Caire, EGY, 23-24 février 1990. Cemagref Editions, Antony, pp.  
843 127-140.
- 844 Lesaffre, B., 1988. Fonctionnement hydrologique et hydraulique du drainage souterrain des  
845 sols temporairement engorgés : débits de pointe et modèle SIDRA : extension des  
846 principes théoriques de Boussinesq et Guyon, 373 p. pp.
- 847 Tournebize, J., Kao, C., Nikolic, N., Zimmer, D., 2004. Adaptation of the STICS model to  
848 subsurface drained soils. Agronomie, 24(6-7): 305-313. DOI:10.1051/agro:2004030
- 849 Henine, H. et al., 2010. Effect of Pipe Pressurization on the Discharge of a Tile Drainage  
850 System. Vadose Zone Journal, 9(1): 36-42. DOI:<https://doi.org/10.2136/vzj2008.0152>

851 Henine, H., Nédélec, Y., Ribstein, P., 2014. Coupled modelling of the effect of overpressure  
852 on water discharge in a tile drainage system. *Journal of Hydrology*, 511: 39-48.  
853 DOI:<https://doi.org/10.1016/j.jhydrol.2013.12.016>

854 Gurovich, L., Oyarce, P., 2015. Modeling agricultural drainage hydraulic nets. *Irrig Drain*  
855 *Syst Eng*, 4: 149-158. DOI:10.4172/2168-9768.1000149

856 Skaggs, R.W., Youssef, M., Chescheir, G.M., 2012. DRAINMOD: model use, calibration,  
857 and validation. *Transactions of the ASABE*, 55: 1509-1522.  
858 DOI:10.13031/2013.42259

859 Valipour, M., 2012. Effect of Drainage Parameters Change on Amount of Drain Discharge in  
860 Subsurface Drainage Systems. *IOSR Journal of Agriculture and Veterinary Science*  
861 (IOSR-JAVS), 1: 10-18. DOI:10.9790/2380-0141018

862 Alzraiee, A.H., Gates, T.K., Garcia, L.A., 2013. Modeling Subsurface Heterogeneity of  
863 Irrigated and Drained Fields. II: Multivariate Stochastic Analysis of Root-Zone  
864 Hydrosalinity and Crop Yield. *Journal of Irrigation and Drainage Engineering*,  
865 139(10): 809-820. DOI:doi:10.1061/(ASCE)IR.1943-4774.0000587

866 Bouarfa, S., 1995. Drainage of irrigated schemes Taking into account the evaporation in  
867 drainage modeling, Université de Strasbourg.

868 Bouarfa, S., Zimmer, D., 2000. Water-table shapes and drain flow rates in shallow drainage  
869 systems. *Journal of Hydrology*, 235(3-4): 264-275. DOI:Doi 10.1016/S0022-  
870 1694(00)00280-8

871 Jeantet, A. et al., 2021. Robustness of a parsimonious subsurface drainage model at the  
872 French national scale. *Hydrol. Earth Syst. Sci.*, 25(10): 5447-5471.  
873 DOI:10.5194/hess-25-5447-2021

874 Henine, H. et al., 2022. Coupling of a subsurface drainage model with a soil reservoir model  
875 to simulate drainage discharge and drain flow start. *Agricultural Water Management*,  
876 262: 107318. DOI:<https://doi.org/10.1016/j.agwat.2021.107318>

877 Blöschl, G. et al., 2019. Twenty-three unsolved problems in hydrology (UPH) – a community  
878 perspective. *Hydrological Sciences Journal*, 64(10): 1141-1158.  
879 DOI:10.1080/02626667.2019.1620507

880 Jiang, Q. et al., 2020. Assessing climate change impacts on greenhouse gas emissions, N  
881 losses in drainage and crop production in a subsurface drained field. *Sci Total*  
882 *Environ*, 705: 135969. DOI:<https://doi.org/10.1016/j.scitotenv.2019.135969>

883 Golmohammadi, G. et al., 2021. Assessment of Impacts of Climate Change on Tile Discharge  
884 and Nitrogen Yield Using the DRAINMOD Model. *Hydrology*, 8(1): 1.  
885 DOI:10.3390/hydrology8010001

886 Stange, F. et al., 2000. A process-oriented model of N<sub>2</sub>O and NO emissions from forest soils:  
887 2. Sensitivity analysis and validation. *Journal of Geophysical Research: Atmospheres*,  
888 105(D4): 4385-4398. DOI:10.1029/1999jd900948

889 Migliaccio, K., Chaubey, I., 2005. Sensitivity Analysis, Calibration, and Validations for a  
890 Multisite and Multivariable SWAT Model. *JAWRA Journal of the American Water*  
891 *Resources Association*, 41: 1077-1089. DOI:10.1111/j.1752-1688.2005.tb03786.x

892 Razavi, S. et al., 2021. The Future of Sensitivity Analysis: An essential discipline for systems  
893 modeling and policy support. *Environmental Modelling & Software*, 137: 104954.  
894 DOI:<https://doi.org/10.1016/j.envsoft.2020.104954>

895 Sobol, I.M., 1993. Sensitivity estimates for nonlinear mathematical models. *Mathematical*  
896 *modelling and computational experiments*, 1(4): 407-414.

897 Saltelli, A., 2002. Making best use of model evaluations to compute sensitivity indices.  
898 *Computer physics communications*, 145(2): 280-297. DOI:10.1016/S0010-  
899 4655(02)00280-1

900 Cacuci, D., 1981. Sensitivity Theory for Nonlinear Systems. I. Nonlinear Functional Analysis  
901 Approach. *Journal of Mathematical Physics*, 22: 2794-2802. DOI:10.1063/1.525186

902 Morris, M.D., 1991. Factorial sampling plans for preliminary computational experiments.  
903 *Technometrics*, 33(2): 161-174. DOI:Doi 10.2307/1269043

904 Kucherenko, S., 2009. Derivative based global sensitivity measures and their link with global  
905 sensitivity indices. *Mathematics and Computers in Simulation*, 79(10): 3009-3017.  
906 DOI:10.1016/j.matcom.2009.01.023

907 Lamboni, M., Iooss, B., Popelin, A.-L., Gamboa, F., 2013. Derivative-based global  
908 sensitivity measures: general links with Sobol'indices and numerical tests.  
909 *Mathematics and Computers in Simulation*, 87: 45-54.  
910 DOI:10.1016/j.matcom.2013.02.002

911 Gejadze, I., Malaterre, P.O., Shutyaev, V., 2019. On the use of derivatives in the polynomial  
912 chaos based global sensitivity and uncertainty analysis applied to the distributed  
913 parameter models. *Journal of Computational Physics*, 381: 218-245.  
914 DOI:10.1016/j.jcp.2018.12.023

915 Michel, C., 1989. *Hydrologie appliquée aux petits bassins versants ruraux*. Cemagref, antony.

916 Mathevet, T., 2005. Quels modèles pluie-débit globaux pour le pas de temps horaire?  
917 Développement empirique et comparaison de modèles sur un large échantillon de  
918 bassins versants. ENGREF (Paris): Cemagref (Antony), France, 463p.

919 Abbaszadeh, P., Moradkhani, H., Daescu, D.N., 2019. The quest for model uncertainty  
920 quantification: A hybrid ensemble and variational data assimilation framework. *Water*  
921 *Resour Res*, 55(3): 2407-2431. DOI:10.1029/2018WR023629

922 Courtier, P. et al., 1998. The ECMWF implementation of three-dimensional variational  
923 assimilation (3D-Var). I: Formulation. *Quarterly Journal of the Royal Meteorological*  
924 *Society*, 124(550): 1783-1807. DOI: <https://doi.org/10.1002/qj.49712455002>

925 Fischer, C., Montmerle, T., Berre, L., Auger, L., Ștefănescu, S.E., 2005. An overview of the  
926 variational assimilation in the ALADIN/France numerical weather-prediction system.  
927 *Quarterly Journal of the Royal Meteorological Society: A Journal of the atmospheric*  
928 *sciences, applied meteorology and physical oceanography*, 131(613): 3477-3492.  
929 DOI:<https://doi.org/10.1256/qj.05.115>

930 Gauthier, P., Tanguay, M., Laroche, S., Pellerin, S., Morneau, J., 2007. Extension of 3DVAR  
931 to 4DVAR: Implementation of 4DVAR at the Meteorological Service of Canada.  
932 *Monthly Weather Review*, 135(6): 2339-2354. DOI:10.1175/mwr3394.1

933 Nguyen, V.T., Georges, D., Besançon, G., Zin, I., 2016. Parameter estimation of a real  
934 hydrological system using an adjoint method\*\*This work has been partially supported  
935 by the LabEx PERSYVAL-Lab (ANR-11-LABX-0025-01) and the MEPIERA  
936 project, Grenoble Institute of Technology. *IFAC-PapersOnLine*, 49(13): 300-305.  
937 DOI:<https://doi.org/10.1016/j.ifacol.2016.07.978>

938 Oubanas, H., Gejadze, I., Malaterre, P.-O., Mercier, F., 2018. River discharge estimation  
939 from synthetic SWOT-type observations using variational data assimilation and the  
940 full Saint-Venant hydraulic model. *Journal of Hydrology*, 559: 638-647.  
941 DOI:10.1016/j.jhydrol.2018.02.004

942 Ghorbanidehno, H., Kokkinaki, A., Lee, J., Darve, E., 2020. Recent developments in fast and  
943 scalable inverse modeling and data assimilation methods in hydrology. *Journal of*  
944 *Hydrology*, 591: 125266. DOI:<https://doi.org/10.1016/j.jhydrol.2020.125266>

945 Jay-Allemand, M. et al., 2020. On the potential of variational calibration for a fully  
946 distributed hydrological model: application on a Mediterranean catchment. *Hydrol.*  
947 *Earth Syst. Sci.*, 24(11): 5519-5538. DOI:10.5194/hess-24-5519-2020

948 Dennis, J., John E, Moré, J.J., 1977. Quasi-Newton methods, motivation and theory. *SIAM*  
949 *review*, 19(1): 46-89. DOI:Doi 10.1137/1019005

950 Arsenault, R., Poulin, A., Côté, P., Brissette, F., 2014. Comparison of stochastic optimization  
951 algorithms in hydrological model calibration. *Journal of Hydrologic Engineering*,  
952 19(7): 1374-1384. DOI:10.1061/(Asce)He.1943-5584.0000938

953 Pan, L., Wu, L., 1998. A hybrid global optimization method for inverse estimation of  
954 hydraulic parameters: Annealing-simplex method. *Water Resour Res*, 34(9): 2261-  
955 2269. DOI:https://doi.org/10.1029/98WR01672

956 Skahill, B.E., Doherty, J., 2006. Efficient accommodation of local minima in watershed  
957 model calibration. *Journal of Hydrology*, 329(1-2): 122-139.  
958 DOI:10.1016/j.jhydrol.2006.02.005

959 Shoarinezhad, V., Wieprecht, S., Haun, S., 2020. Comparison of Local and Global  
960 Optimization Methods for Calibration of a 3D Morphodynamic Model of a Curved  
961 Channel. *Water*, 12(5): 1333. DOI:10.3390/w12051333

962 Welter, D.E. et al., 2012. Approaches in highly parameterized inversion - PEST++, a  
963 Parameter ESTimation code optimized for large environmental models. 7-C5, Reston,  
964 VA. DOI:10.3133/tm7C5

965 Beven, K., 2006. A manifesto for the equifinality thesis. *Journal of Hydrology*, 320(1): 18-36.  
966 DOI:10.1016/j.jhydrol.2005.07.007

967 Goutal, N. et al., 2018. Uncertainty Quantification for River Flow Simulation Applied to a  
968 Real Test Case: The Garonne Valley, pp. 169-187. DOI:10.1007/978-981-10-7218-  
969 5\_12

970 Tallec, G., 2012. 1962-2012 : cinquante ans d'observations, un bien précieux pour la  
971 recherche et les services opérationnels. *Sciences Eaux & Territoires, Cahier*  
972 *spécial(III)*: 2-9. DOI:10.3917/set.hs05.0002

973 FAO, F., 2006. Agriculture Organization of the United Nations (2006) Guidelines for Soil  
974 Description, ISBN 92-5-105521-1.

975 Tournebize, J. et al., 2015. Long-term nitrate removal in a buffering pond-reservoir system  
976 receiving water from an agricultural drained catchment. *Ecological Engineering*, 80:  
977 32-45. DOI:10.1016/j.ecoleng.2014.11.051

978 Vidal, J.-P., Martin, E., Franchistéguy, L., Baillon, M., Soubeyroux, J.-M., 2010. A 50-year  
979 high-resolution atmospheric reanalysis over France with the Safran system.  
980 *International Journal of Climatology*, 30(11): 1627-1644.  
981 DOI:https://doi.org/10.1002/joc.2003

982 Hooghoudt, S., 1940. General consideration of the problem of field drainage by parallel  
983 drains, ditches, watercourses, and channels. Contribution to the knowledge of some  
984 physical parameters of the soil, 7.

985 Augeard, B., Kao, C., Chaumont, C., Vauclin, M., 2005. Mechanisms of surface runoff  
986 genesis on a subsurface drained soil affected by surface crusting: A field  
987 investigation. *Physics and Chemistry of the Earth*, 30(8): 598-610.  
988 DOI:10.1016/j.pce.2005.07.014

989 Hascoet, L., Pascual, V., 2013. The Tapenade Automatic Differentiation tool: principles,  
990 model, and specification. *ACM Transactions on Mathematical Software*, 39(3).  
991 DOI:10.1145/2450153.2450158

992 Gupta, H.V., Kling, H., Yilmaz, K.K., Martinez, G.F., 2009. Decomposition of the mean  
993 squared error and NSE performance criteria: Implications for improving hydrological  
994 modelling. *Journal of Hydrology*, 377(1): 80-91.  
995 DOI:https://doi.org/10.1016/j.jhydrol.2009.08.003

996 Pechlivanidis, I., Jackson, B., Mcintyre, N., Wheeler, H., 2011. Catchment scale hydrological  
997 modelling: a review of model types, calibration approaches and uncertainty analysis  
998 methods in the context of recent developments in technology and applications. *Global*  
999 *NEST journal*, 13(3): 193-214.

1000 Patil, S.D., Stieglitz, M., 2015. Comparing spatial and temporal transferability of  
1001 hydrological model parameters. *Journal of Hydrology*, 525: 409-417.  
1002 DOI:https://doi.org/10.1016/j.jhydrol.2015.04.003

1003 Haas, M.B., Guse, B., Pfannerstill, M., Fohrer, N., 2016. A joined multi-metric calibration of  
1004 river discharge and nitrate loads with different performance measures. *Journal of*  
1005 *Hydrology*, 536: 534-545. DOI:https://doi.org/10.1016/j.jhydrol.2016.03.001

1006 Santos, L., 2018. Perspectives for hydrological supermodels: evaluation of a method based on  
1007 a dynamical combination of rainfall-runoff models, Doctorat en Hydrologie,  
1008 AgroParisTech, 256 pp.

1009 Reichle, R.H., 2008. Data assimilation methods in the Earth sciences. *Advances in Water*  
1010 *Resources*, 31(11): 1411-1418. DOI:https://doi.org/10.1016/j.advwatres.2008.01.001

1011 Perrin, C., Michel, C., Andréassian, V., 2003. Improvement of a parsimonious model for  
1012 streamflow simulation. *Journal of hydrology*, 279(1-4): 275-289.  
1013 DOI:10.1016/S0022-1694(03)00225-7

1014 Coron, L., Thirel, G., Delaigue, O., Perrin, C., Andréassian, V., 2017. The suite of lumped  
1015 GR hydrological models in an R package. *Environmental modelling & software*, 94:  
1016 166-171. DOI:10.1016/j.envsoft.2017.05.002

1017 Gejadze, I., Malaterre, P.-O., 2017. Discharge estimation under uncertainty using variational  
1018 methods with application to the full Saint-Venant hydraulic network model.  
1019 *International Journal for Numerical Methods in Fluids*, 83(5): 405-430.  
1020 DOI:10.1002/flid.4273

1021 Zhu, C., Byrd, R.H., Lu, P., Nocedal, J., 1997. Algorithm 778: L-BFGS-B: Fortran  
1022 subroutines for large-scale bound-constrained optimization. *ACM Transactions on*  
1023 *Mathematical Software (TOMS)*, 23(4): 550-560. DOI:Doi 10.1145/279232.279236

1024 Tremolet, Y., 2006. Accounting for an imperfect model in 4D-Var. *Quarterly Journal of the*  
1025 *Royal Meteorological Society: A journal of the atmospheric sciences, applied*  
1026 *meteorology and physical oceanography*, 132(621): 2483-2504.  
1027 DOI:10.1256/qj.05.224

1028 Beal, M.J., 2003. Variational algorithms for approximate Bayesian inference. University of  
1029 London, University College London (United Kingdom).

1030 Duan, Q., Sorooshian, S., Gupta, V., 1992. Effective and efficient global optimization for  
1031 conceptual rainfall-runoff models. *Water Resour Res*, 28(4): 1015-1031. DOI:Doi  
1032 10.1029/91wr02985

1033 Klemeš, V., 1986. Operational testing of hydrological simulation models. *Hydrological*  
1034 *Sciences Journal*, 31(1): 13-24. DOI:10.1080/02626668609491024

1035 Henriksen, H.J. et al., 2003. Methodology for construction, calibration and validation of a  
1036 national hydrological model for Denmark. *Journal of Hydrology*, 280(1): 52-71.  
1037 DOI:https://doi.org/10.1016/S0022-1694(03)00186-0

1038 Guo, D., Zheng, F., Gupta, H., Maier, H.R., 2020. On the Robustness of Conceptual Rainfall-  
1039 Runoff Models to Calibration and Evaluation Data Set Splits Selection: A Large  
1040 Sample Investigation. *Water Resour Res*, 56(3): e2019WR026752.  
1041 DOI:https://doi.org/10.1029/2019WR026752

1042 Kenney, J.F., 1939. *Mathematics of statistics*. D. Van Nostrand.

1043 Nash, J.E., Sutcliffe, J.V., 1970. River flow forecasting through conceptual models part I—A  
1044 discussion of principles. *Journal of hydrology*, 10(3): 282-290.  
1045 DOI:https://doi.org/10.1016/0022-1694(70)90255-6

1046 Lagacherie, P., 1987. Synthèse générale sur les études de secteur de référence drainage,  
1047 irstea.

- 1048 Iooss, B., Lemaître, P., 2015. A review on global sensitivity analysis methods, Uncertainty  
1049 management in simulation-optimization of complex systems. Springer, pp. 101-122.  
1050 DOI:10.1007/978-1-4899-7547-8\_5
- 1051 Zhang, X.Y., Trame, M.N., Lesko, L.J., Schmidt, S., 2015. Sobol Sensitivity Analysis: A  
1052 Tool to Guide the Development and Evaluation of Systems Pharmacology Models.  
1053 CPT Pharmacometrics Syst Pharmacol, 4(2): 69-79. DOI:10.1002/psp4.6
- 1054 Viana, F.A.C., 2016. A Tutorial on Latin Hypercube Design of Experiments. Quality and  
1055 Reliability Engineering International, 32(5): 1975-1985.  
1056 DOI:https://doi.org/10.1002/qre.1924
- 1057 Manache, G., Melching, C.S., 2004. Sensitivity Analysis of a Water-Quality Model Using  
1058 Latin Hypercube Sampling. Journal of Water Resources Planning and Management,  
1059 130(3): 232-242. DOI:doi:10.1061/(ASCE)0733-9496(2004)130:3(232)
- 1060 Zimmer, D., Lorre, E., Lesaffre, B., 1995. Parameter sensitivity and field evaluation of  
1061 SIDRA model. Irrigation and Drainage Systems, 9(3): 279-296.  
1062 DOI:10.1007/BF00880868
- 1063 Jamagne, M., Betremieux, R., Begon, J.C., Mori, A., 1977. Quelques données sur la  
1064 variabilité dans le milieu naturel de la réserve en eau des sols. Bulletin Technique  
1065 d'Information, 324-325: 627-641.
- 1066 Goulet, E., Morlat, R., Rioux, D., Cesbron, S., 2004. A calculation method of available soil  
1067 water content : application to viticultural terroirs mapping of the Loire valley. OENO  
1068 One, 38(4): 231-235. DOI:10.20870/oenone.2004.38.4.913
- 1069 Antoulas, A.C., 2005. Approximation of large-scale dynamical systems. SIAM.  
1070 DOI:https://doi.org/10.1137/1.9780898718713
- 1071 Altaf, M.U., El Gharamti, M., Heemink, A.W., Hoteit, I., 2013. A reduced adjoint approach  
1072 to variational data assimilation. Computer Methods in Applied Mechanics and  
1073 Engineering, 254: 1-13. DOI:10.1016/j.cma.2012.10.003
- 1074 LeGresley, P., Alonso, J., 2000. Airfoil design optimization using reduced order models  
1075 based on proper orthogonal decomposition, Fluids 2000 Conference and Exhibit.  
1076 DOI:10.2514/6.2000-2545
- 1077 Turunen, M., Gurarslan, G., Šimůnek, J., Koivusalo, H., 2020. What is the worth of drain  
1078 discharge and surface runoff data in hydrological simulations? Journal of Hydrology:  
1079 125030. DOI:https://doi.org/10.1016/j.jhydrol.2020.125030
- 1080 Hoteit, I., 2008. A reduced-order simulated annealing approach for four-dimensional  
1081 variational data assimilation in meteorology and oceanography. International Journal

1082 for Numerical Methods in Fluids, 58(11): 1181-1199.  
1083 DOI:<https://doi.org/10.1002/flid.1794>  
1084 Chossat, J.C., Saugnac, A.M., 1985. Relation entre conductivité hydraulique et porosité de  
1085 drainage mesurées par la méthode du puits et des piézomètres. Sciences du sol(3):  
1086 151-167.  
1087

1088 **APPENDIX A**

1089 **A.1. calculation of the corrected evapotranspiration (CET)**

Case 1: If  $(S(t) > 0.6 * S_{inter})$        $CET = \beta * PET$   
 1090 Case 2: If  $(S(t) < 0.6 * S_{inter})$        $CET = \beta * PET * \exp\left(-\frac{0.6*S_{inter} - S(t)}{S(t)}\right)$       (A.1)  
 Case 3: If  $(S(t) < 0)$        $CET = 0$

1091 **A.2. Recharge (R) and water level in the soil reservoir (S) calculation**

Case 1: If  $(0 < S(t) < S_{inter})$        $S(t) = S(t - 1) + (P - CET);$        $R(t) = 0$   
 1092 Case 2: If  $(S_{inter} < S(t) < S_{max})$        $S(t) = S(t - 1) + (1 - \alpha) * (P - CET);$        $R(t) = \alpha * (P - CET)$       (A.2)  
 Case 3: If  $(S(t) < 0)$        $S(t) = 0;$        $R(t) = \alpha * (P - CET)$

1093 **A.3. Water table level and discharge calculation**

1094  $h(t) = h(t - 1) + \left(R(t) - K_{sat} \frac{h(t-1)^2}{l^2}\right) / \mu C$   
 $Q(t) = AJ(h(t)) + (1 - A)R(t)$       (A.3)  
 $J(h(t)) = K_{sat} \frac{h(t)^2}{l^2}$